Transfer RNA Genes Affect Chromosome Structure and Function via Local Effects

Omar Hamdani[1*], Namrita Dhillon[1*], Tsung-Han S. Hsieh[3*], Takahiro Fujita[4*], Josefina Ocampo[5*], Jacob G. Kirkland[1], Josh Lawrimore[6], Tetsuya J. Kobayashi[7], Brandon Friedman[6], Derek Fulton[6], Kenneth Y. Wu[1], Răzvan V. Chereji[5], Masaya Oki[4], Kerry Bloom[6], David J Clark[5], Oliver J. Rando[3], Rohinton T. Kamakaka[1,2]

1 Department of MCD Biology**,** 1156 High Street, University of California, Santa Cruz, CA 95064 USA
E-mail: rohinton@ucsc.edu

2 Corresponding Author

3 Department of Biochemistry and Molecular Pharmacology, University of Massachusetts Medical School, Worcester, MA 01605, USA
4 Department of Applied Chemistry Biotechnology, University of Fukui, Bunkyo, Fukui, Japan.
5 Division of Developmental Biology, Eunice Kennedy Shriver National Institute of Child Health and Human Development, 6 Center Drive, Bethesda MD 20892 USA
6 Department of Biology, University of North Carolina at Chapel Hill, Chapel Hill, NC 27599-3280 USA
7 Institute of Industrial Science, The University of Tokyo, Tokyo, Japan

* These authors contributed equally

Abstract

The genome is packaged and organized in an ordered, non-random manner and specific chromatin segments contact nuclear substructures to mediate this organization. While transfer RNA genes (tDNAs) are essential for the generation of tRNAs, these loci are also binding sites for transcription factors and architectural proteins and are thought to play an important role in the organization of the genome. In this study, we investigate the role of tDNAs in genomic organization and chromosome function by editing a chromosome so that it lacks any tDNAs. Surprisingly our analyses of this tDNA-less chromosome show that loss of tDNAs does not grossly affect chromosome folding or chromosome tethering. However, loss of tDNAs affects local nucleosome positioning and the binding of SMC proteins at these loci. The absence of tDNAs also leads to changes in centromere clustering and a reduction in the frequency of long range *HML*-*HMR* heterochromatin clustering. We propose that the tDNAs primarily affect local chromatin structure that result in effects on long-range chromosome architecture.

Introduction

The three dimensional organization of the yeast nucleus is non-random (Reviewed in (Taddei et al., 2010; Zimmer and Fabre, 2011)). Each chromosome occupies a specific territory in the nucleus anchored to nuclear substructures via specific DNA sequences. The telomeres of each chromosome tend to associate with one another and with the nuclear envelope in small clusters, based on the length of the chromosome arms (Fabre and Spichal, 2014; Palladino et al., 1993b; Ruben et al., 2011). The rDNA repeats on chromosome XII are packaged into a dense structure known as the nucleolus, which also localizes to the nuclear periphery (Oakes et al., 1998). Opposite the nucleolus is the spindle pole body, which is the interphase attachment site for the centromeres of the 16 chromosomes (Jin et al., 2000). Attachment of centromeres to the spindle pole and attachment of telomeres to the nuclear membrane dependent upon chromosome arm length helps organize the nucleus (Therizols et al., 2010). The active genes along the chromosome arms primarily reside in the nuclear interior though some active genes including some tRNA genes interact with nuclear pores and help tether the arms (Duan et al., 2010; Taddei et al., 2010; Tjong et al., 2012).

Besides DNA sequence elements, numerous proteins play a role in nuclear organization via networks of interactions between nuclear membrane and chromatin bound proteins. Chromatin bound proteins involved in this organization include heterochromatin proteins, (Palladino et al., 1993a), lamin like proteins (Andrulis et al., 2002; Bupp et al., 2007; Mekhail et al., 2008; Taddei et al., 2005; Taddei et al., 2004), specific transcription factors (Klein et al., 1992; Taddei et al., 2006), RNA polymerases

(Oakes et al., 1998) and DNA repair proteins (Kirkland et al., 2015; Kirkland and Kamakaka, 2013) (see (Taddei et al., 2010) for review).

tRNA genes (tDNAs) are a class of active genes found on all chromosomes and are bound by transcription factors TFIIIB and TFIIIC and RNA polymerase III. tDNAs are short, highly transcribed DNA sequences (Dieci et al., 2007) that are usually nucleosome-free with strongly positioned flanking nucleosomes (Cole et al., 2012; Oki and Kamakaka, 2005; Weiner et al., 2010; Yuan et al., 2005). The tDNAs contain internal promoter elements called A and B-boxes, which aid in the binding of the transcription factor TFIIIC (Geiduschek and Kassavetis, 2001; Schramm and Hernandez, 2002). TFIIIC helps recruit TFIIIB to AT rich sequences upstream of the tDNA. tDNA-bound transcription factors function via interactions with cofactors. tRNA genes are sites of binding for numerous chromatin proteins including the architectural SMC proteins, nuclear pore proteins, chromatin remodelers and histone modifiers. Studies from several labs have shown that tDNAs are enriched in cohesin (Smc1/Smc3) (Glynn et al., 2004), and condensin (Smc2/Smc4) complexes (D'Ambrosio et al., 2008; Haeusler et al., 2008), as well as the SMC loading proteins (Scc2/Scc4) (Kogut et al., 2009; Lopez-Serra et al., 2014) and some chromatin remodelers including RSC (Bausch et al., 2007; D'Ambrosio et al., 2008; Dhillon et al., 2009; Huang and Laurent, 2004; Oki and Kamakaka, 2005).

While individual tRNA genes turn over rapidly as a result of mutational inactivation and gene loss (Frenkel et al., 2004; Goodenbour and Pan, 2006; Withers et al., 2006), a subset of tDNA are syntenic with respect to neighboring sequences (Raab et al., 2012; Wang et al., 2012) and data suggest that these conserved tDNAs possess chromosome

102 position-specific functions in gene regulation (reviewed in (Kirkland et al., 2013; Van
103 Bortle and Corces, 2012)). There are several position-specific effects mediated by
104 tDNAs. First, tDNAs have been shown to function as heterochromatin barrier insulators,
105 which stop the spread of heterochromatic domains into adjacent non-silenced domains
106 (Biswas et al., 2009; Dhillon et al., 2009; Donze et al., 1999; Raab et al., 2012). Second,
107 tDNAs block communication between enhancers and promoters when located between
108 these elements in yeast, *Drosophila*, mouse and human cells by acting as enhancer
109 blockers (Dixon et al., 2012; Ebersole et al., 2011; Korde et al., 2013; Raab et al., 2012;
110 Simms et al., 2008; Simms et al., 2004; Van Bortle et al., 2014). Third, the presence of
111 a tDNA in close proximity to a RNA pol II transcribed gene promoter antagonizes
112 transcription from the pol II transcribed gene in a phenomenon refereed to as tRNA
113 gene mediated silencing (tgm silencing) (Good et al., 2013; Haeusler et al., 2008;
114 Thompson et al., 2003).

115 In many organisms, tDNAs have also been shown to cluster at sites in the nucleus
116 (Haeusler and Engelke, 2006; Iwasaki et al., 2010; Kirkland et al., 2013; Pombo et al.,
117 1999; Raab et al., 2012). In *S. cerevisiae*, DNA FISH studies have shown that some
118 tDNAs cluster together adjacent to centromeres (Haeusler and Engelke, 2006;
119 Thompson et al., 2003) while proximity ligation analysis suggest that tDNAs cluster at
120 the outer periphery of the nucleolus as well as near the centromeres (Duan et al., 2010)
121 though more recent HiC studies seem unable to detect these long-range associations
122 (Schalbetter bioRxiv 094946). Based on these results it has been proposed that TFIIIC
123 binding to discrete sites along the chromosome plays an important role in chromosome

124 folding and organization in the yeast nucleus (Haeusler and Engelke, 2004, 2006;
125 Iwasaki and Noma, 2012).

126 To better analyze the role of tDNAs in chromatin looping and organization we
127 generated a “tDNA-less” chromosome through the systematic deletion of all the tDNAs
128 on chromosome III in *S. cerevisiae*. We characterized chromatin packaging,
129 chromosome folding and nuclear dynamics of this chromosome. We show that tDNA
130 loss affects nucleosome positioning and loading of SMC proteins in the vicinity of tDNAs
131 but this has no effect on chromatin looping. While loss of the tDNAs does not affect
132 chromatin looping, it does affect centromere clustering and the long-range interactions
133 of the silenced *HML* and *HMR* loci with concomitant effects on gene silencing.
134

Results

The ~275 tDNAs in the budding yeast genome are dispersed across all 16 chromosomes. Here, we focus on chromosome III, which is 316 kb long and has two tDNAs on the left arm and eight tDNAs on the right arm. In order to investigate the role of tDNAs in chromatin looping, nuclear organization and function, we created a strain in which chromosome III is devoid of any functional tDNAs by deleting an internal fragment of each tDNA. The deletions eliminate the internal promoter elements (both BoxA and BoxB) and thus eliminate the binding of the transcription factors TFIIIC and TFIIIB. For simplicity, we have labeled the tDNA adjacent to the *HMR* locus as t0 and have labeled the remaining nine tDNAs going from right to left as t1, t2, t3 etc. (Figure 1). To delete the tDNAs we first replaced an internal segment of the gene with a *URA3* gene and then subsequently replaced *URA3* with a DNA fragment containing a unique DNA barcode. This involved multiple sequential transformations. Each deletion was monitored by PCR analysis, and intermediate strains were backcrossed to wild type W-303 prior to additional rounds of transformations. All of the experiments described were performed in this strain background to avoid strain specific effects.

Most tRNA isoacceptor families have multiple copies, scattered throughout the genome, though single gene copies code for six isoacceptor families. On chromosome III eight of the ten tDNAs that were deleted are members of multi-copy gene families (with 10-16 copies in the genome) and are not essential. However, tDNA t1 (*tS(CGA)c*) is a single copy gene and is essential in *S. cerevisiae* (Ho and Abelson, 1988) and there are only two copies of tDNA t7 (*tP(AGG)c*) in the genome. Loss of t7 from chromosome III caused cells to grow more slowly. In order to remove these two genes from

158 chromosome III and simultaneously maintain the health of the yeast, we integrated
159 single copies of these two genes on chromosome XV at the *HIS3* locus. Once the full
160 tDNA deletion chromosome III had been constructed, the strain harboring this
161 chromosome was backcrossed with wild-type W-303, and segregation of the deleted
162 tDNAs was monitored by PCR using primers specific to the unique barcodes. The full-
163 length sequence of this modified chromosome is available.

164 The strain where chromosome III lacked any tDNAs (tDNA delete) was grown in
165 rich media at 30C and did not show any obvious growth defect, forming homogeneous
166 and healthy, smooth edged colonies. Strains bearing this tDNA-less chromosome had a
167 doubling time of ~90 minutes in liquid YPD media, which was indistinguishable from a
168 wild type strain. This is consistent with data showing that loss of one copy of multi-copy
169 tDNAs in yeast cells do not lead to growth defects in rich media (Bloom-Ackermann et
170 al., 2014). Qualitative chromosome loss assays in a homozygous diploid strain, based
171 on the appearance of pseudo-haploids capable of mating, showed no change in
172 chromosome loss rates indicating that chromosome segregation during mitosis had not
173 been perturbed.

174 **Changes to the local nucleosome landscape surrounding the tDNAs**

175 The stable binding of TFIIIC and TFIIIB as well as their interactions with chromatin
176 remodelers result in nucleosome eviction at the tDNA and positioning of nucleosomes
177 adjacent to the gene (Dion et al., 2007; Oki and Kamakaka, 2005). At some tRNA genes
178 a single nucleosome appears to be disrupted while at other tDNAs multiple
179 nucleosomes are disrupted. Since tDNAs are dispersed across the chromosome and
180 are highly transcribed we first asked if loss of all ten tDNAs from the chromosome

181 altered the nucleosome and transcription landscape of the chromosome. In order to
182 determine if tDNAs affect nucleosome positions across chromosome III, we mapped
183 nucleosomes in our tDNA delete strain as well as in the wild type strain.
184 Haploid yeast cells were grown to log phase, harvested and nuclei were digested
185 with varying concentrations of micrococcal nuclease to generate mono-nucleosome
186 protected DNAs, which were subjected to paired-end MNase-seq. Overall, the
187 nucleosome landscape across all chromosomes except chromosome III was unaffected
188 by the presence or absence of the chromosome III tDNAs. More focused analysis
189 showed no change in nucleosome positioning in the proximity of the 265 tDNAs
190 scattered on the 15 chromosomes that were not manipulated in this study (Figure 2 left
191 panel).
192 In contrast, changes in nucleosome occupancy were observed at or immediately
193 adjacent to the deleted tDNAs on chromosome III. Figure 2 (right panel) shows the
194 average nucleosome occupancy across 2kb segments centered on the chromosome III
195 tDNAs with each tDNA in WT cells aligned at its 5' end while in the tDNA delete strain,
196 the 5' ends of the deletion points were aligned. In the wild type strain there is a clear
197 nucleosome free region centered on the tDNA flanked by positioned nucleosomes
198 reflecting differential digestion of the TFIIIB-TFIIIC complex relative to nucleosomes
199 (Chereji et al., 2017). In the tDNA delete strain this pattern is altered and a nucleosome
200 is usually formed over the deletion junction (see Supplementary figure 1). We were
201 unable to determine the change in the chromatin landscape around t1 and t7 tDNAs
202 since these two genes with 100 bp of flanking sequences were transposed to the *HIS3*
203 locus. Nucleosome positions elsewhere on chromosome III that are distant from the

tDNAs are not altered on the tDNA-less chromosome (Supplementary figure 2). These results demonstrate that tDNAs create nucleosome free regions at the tRNA gene with positioned nucleosomes flanking the gene. The data also show that their chromatin organizing effects are locally confined and do not extend beyond their immediate vicinity.

tDNA loss affects expression of very few RNA pol II transcribed genes

The presence of a tDNA in close proximity to a RNA pol II transcribed gene promoter antagonizes transcription from the pol II transcribed gene called tRNA gene mediated silencing (tgm silencing) (Good et al., 2013; Haeusler et al., 2008; Thompson et al., 2003). In addition, tDNAs have also been shown to function as enhancer blockers when located between an UAS enhancer and a promoter (Simms et al., 2008). Since the loss of the tDNAs altered nucleosomes in their vicinity we wondered if these alterations affected the transcription landscape of genes on chromosome III. Rather than restrict the analysis to pol II transcribed genes adjacent to the tDNAs on chromosome III, we investigated the effects of tDNA loss on all pol II transcribed genes in the genome and analyzed the changes in RNA levels in the wild type and tDNA delete strain by RNA-seq. Total RNA was extracted from exponentially growing yeast cultures and RNA-seq libraries were prepared, sequenced and analyzed as described in the materials and methods section. The RNA levels of a very small number of genes were affected upon deletion of the tDNAs. Table1 lists the genes that were either up regulated or down regulated in the strain lacking tDNAs on chromosome III. Of the ten tDNAs present on chromosome III, tDNA t0, t8 and t9 are flanked by retrotransposon elements and since these are repetitive elements, the tDNA-mediated transcription effects could not be

investigated for these loci. Furthermore, tDNAs t3 and t4 are missing in W-303. The expression of only two genes on chromosome III was affected and in both instances, a tDNA (t1 and t6) was located adjacent to the gene. In one instance the gene was up regulated upon tDNA loss while in the second instance the gene was down regulated. Furthermore, we observed the up regulation of the *MRM1* gene. This gene resides immediately adjacent to *HIS3*. The tDNAs for t1 and t7 were ectopically inserted at the *HIS3* locus in the tDNA delete strain demonstrating that the ectopic insertion of the tDNAs is the cause of the change in expression of *MRM1*. These data suggest that tDNA mediated position effects are highly context dependent and only affect some pol II transcribed genes and not others.

Of the genes that were down regulated in the tDNA delete strain, several are involved in amino acid biosynthesis though these genes are scattered throughout the genome and do not localize near tDNAs. The reason why expression of these genes was reduced is unclear given that the two yeast strains used are isogenic with respect to nutritional markers, and there are between 10 and 16 copies of each of the six deleted tDNAs in the genome (t0=11 copies, t2=10 copies, t5=16 copies, t6=11 copies, t8=10 copies and t9=15 copies). It is possible that there is a reduction in transcript levels of these genes due to the small reduction in tDNA copy number without any other cell phenotype. This is consistent with a recent study where single tDNAs in yeast were deleted and these single deletions in multi-copy tDNA families also led to changes in the expression of a small set of genes involved in translation (Bloom-Ackermann et al., 2014).

Scc2 binding at tDNAs is dependent upon a functional tDNA but other binding sites are tDNA independent

The SMC proteins play an important role in nuclear organization (Uhlmann, 2016) and tDNAs are major binding sites for SMC proteins and the SMC loaders Scc2/Scc4 and Rsc.. Our nucleosome mapping data indicated that loss of the tDNAs altered nucleosome positions at tDNAs. Since nucleosome free tDNAs are sites for the recruitment of RSC and Scc2/Scc4 proteins (Damelin et al., 2002; Huang and Laurent, 2004; Lopez-Serra et al., 2014; Parnell et al., 2008), we asked if loss of all the tDNAs on chromosome III reduced recruitment of Scc2 proteins at these loci and whether it also affected loading of Scc2 at other sites along the chromosome.

We performed a ChIP-seq of Myc-tagged Scc2 to compare the distribution of this protein genomewide in the WT and tDNA delete strain (Figure 3). This analysis showed that Scc2 bound multiple sites along the chromosome including tDNAs. At some tDNAs the Scc2 binding is focused forming a sharp peak while at other tDNAs the binding is spread over a greater region. Comparison between the wild type and tDNA delete strain showed that Scc2 levels did not decrease at any of the sites on the 15 chromosomes. Upon tDNA loss Scc2 binding decreased at the tDNA loci on chromosome III or at sites in the immediate vicinity of tDNAs such as *LEU2* (adjacent to tDNA t8) (Figure 3 and Supplementary Figure 3) and *HMR* (adjacent to t0). On chromosome III the analysis also showed that there was no significant change in Scc2 binding at other non-tDNA sites. For example we saw a large peak of Scc2 binding at Tel3L. This peak at Tel3L was unchanged upon tDNA deletion (Supplementary Figure4) and similarly we did not

record any change in Scc2 levels at *CEN3* (Supplementary Figure4) confirming that tDNAs are not the sole determinants for the recruitment of Scc2 to chromosomes.

We confirmed this result by ChIP-qPCR against Scc2. A site at the *OCA4* gene was used as an internal control since this site does not bind Scc2 in wild type cells. We were unable to design unique primers at t6 due to the presence of repetitive sequences in the immediate vicinity of this gene and therefore could not map the localization of these proteins at this tDNA. Some primer pairs flank the tDNAs while others are adjacent to the tDNAs. Consistent with the ChIP-Seq data, in wild type cells, Scc2 is enriched at several of the tDNAs present on chromosome III (Figure 4A). We observed ~3.5 fold enrichment at t8 and ~2.5 enrichment at t0, t2 and t5. When the same protein was mapped in the tDNA delete strain we observed a significant reduction in Scc2 binding at these tDNAs. The levels dropped to those observed for the negative control *OCA4* except for the t8 tDNA, where the level dropped two fold but there was some residual Scc2 still present (Figure 4A). The amount of Scc2 did not change at *CEN3* when the tDNAs were absent from the chromosome, indicating that the binding of Scc2 to the centromere was independent of the tDNAs.

Scc2, in association with Scc4 helps recruit the SMC proteins to chromatin (D'Ambrosio et al., 2008; Kogut et al., 2009). Condensins localize to tDNAs and are necessary for the clustering of tDNAs in the nucleus (D'Ambrosio et al., 2008; Haeusler et al., 2008). We therefore mapped the binding of condensins at tDNAs on chromosome III using the HA-tagged Brn1 subunit. In wild type cells, the Brn1 profile was very similar to that previously observed for Scc2 with significant binding of Brn1 at

293 specific tDNAs. Correspondingly, the binding of the condensins was significantly
294 reduced at these sites upon deletion of the tDNA promoters (Figure 4B).

295 **Chromosome mobility on the tDNA-less chromosome**

296 TFIIIC binding sites and tDNAs are described as chromosome organizing clamps
297 because of their consistent association with specific landmarks within the nucleus
298 (Haeusler and Engelke, 2006). The localization of tDNAs with the kinetochore is
299 dependent upon condensins while the interactions of tDNAs with nuclear pores are
300 dependent upon cohesins. These associations likely help tether the chromosome. Since
301 loss of tDNAs from chromosome III led to a decrease in SMC proteins from these sites
302 we wondered if this loss would affect chromosome tethering and mobility of the
303 chromosome. To assess mobility we fluorescently-labeled specific sites on chromosome
304 III, and used these to monitor chromosome mobility in the wild type and the tDNA
305 deletion chromosomes. The location of a point on the chromosome was mapped in
306 three-dimensional space over a defined period of time in relation to another point within
307 the nucleus- the spindle pole body (marked with the Spc29-RFP fusion protein)- and
308 mobility was characterized by mean square distance analysis (MSD) (Dion et al., 2012;
309 Mine-Hattab and Rothstein, 2012; Verdaasdonk et al., 2013). Six chromosomal loci
310 across chromosome III were assayed (Figure 5). These loci were tagged by inserting
311 LacO arrays at these sites and monitored using a LacI-GFP fusion protein mediated
312 fluorescence. Time-lapse movies of individual unbudded cells in the G1 phase of the
313 cell cycle were imaged over the course of 10 minutes. Using this information, MSD
314 curves were generated for each locus in both the WT and tDNA delete strain
315 (Supplementary Figure 4). For the wild type chromosome III, *CEN3* was the most

316 constrained locus (Rc=415 nm), with loci located further from the centromere exhibiting
317 greater mobility. For example, *LEU2*, which is approximately 30kb from the centromere,
318 had an Rc of 522nm while *HMR*, which is approximately 180kb from the centromere,
319 had an Rc value of 688nm. This is consistent with previous data showing that the
320 location of a locus in relation to the centromere is critical in determining its mobility, with
321 loci closer to the centromere displaying decreased mobility compared to loci farther from
322 the centromere (Albert et al., 2013; Tjong et al., 2012; Verdaasdonk et al., 2013). Out of
323 the six loci assayed, none of the loci showed a statistically significant change in mobility
324 following the loss of tDNAs (p values range from 0.15 to 0.75). The data indicate that
325 tDNAs are not major determinants in constraining chromosome segment motion or that
326 they are a subset of factors involved and the redundancy precludes observation of their
327 function.

328 **tDNAs are not required for proper chromatin folding**

329 Transfer RNA genes have been proposed to affect chromatin fiber folding via the
330 clustering of dispersed tRNA genes. The promoters in tDNAs are the binding site for the
331 transcription factor TFIIIC and foci comprised of multiple TFIIIC-bound sites have been
332 proposed to function in chromatin looping and folding (Duan et al., 2010; Haeusler and
333 Engelke, 2004, 2006; Iwasaki and Noma, 2012; Noma et al., 2006; Pombo et al., 1999;
334 Raab et al., 2012; Thompson et al., 2003). If tDNAs are major drivers of chromatin
335 folding and looping, then elimination of these loci from an entire chromosome should
336 lead to changes in the folding of the chromatin fiber or result in changes in chromosome
337 packaging in the nucleus. We set out to determine the detailed three-dimensional
338 organization of chromosome III lacking functional tDNAs. We used a modified

chromosome conformation capture technique called Micro-C XL (Hsieh et al., 2015; Hsieh et al., 2016). We chose Micro-C XL over HiC because it can capture both short length 3D interactions as well as long-length interactions and the method is not dependent upon the presence of restriction sites along the DNA. In brief, yeast cells were first cross-linked with formaldehyde and DSG, and chromatin was then fragmented into mono-nucleosomes via micrococcal nuclease digestion. Cross-linked, digested chromatin was ligated to capture chromosomal interactions. Size-selected ligation products were then purified and subjected to paired-end high-throughput sequencing. Sequencing reads were mapped back to the reference genome to determine the interacting regions of the chromosome, as previously described (Supplementary Figure 5). Overall, Micro-C maps for wild type and tDNA mutant strains both exhibited previously described features of yeast chromosome folding, with no difference in chromatin folding between the tDNA delete and wild type strains. For example, ~2-10kb contact domains (CIDs/TADs) encompassing ~1-5 genes were observed, across all 16 chromosomes, in the wild type strain. Inspection of the chromosome III in the tDNA delete cells showed that these domains persisted even upon loss of the tDNAs (Figure 6). There was no significant change in the contact frequency versus genomic distance in the two strains, indicating no local chromatin decondensation or change in chromatin looping interactions. Thus, tDNAs do not appear to be responsible for the general folding of the chromatin fiber.

tDNAs affect CEN-CEN interaction frequency

While the overall folding of the chromatin fiber of chromosome III was not altered in the absence of tDNAs, and although Scc2 levels were unchanged at centromeres,

Micro-C analysis identified changes in contact frequency at centromeres (Figure 7). The 16 centromeres in yeast are in close physical proximity to one another and cluster adjacent to the spindle pole body (Guacci et al., 1997; Jin et al., 1998; Jin et al., 2000). These CEN-CEN interactions are readily captured by 3C methods including HiC and Micro-C XL (Dekker et al., 2002; Duan et al., 2010; Hsieh et al., 2015), and are recapitulated in this study in the W-303 strain background. Interestingly compared to the wild type strain, the centromere of chromosome III in the tDNA delete strain showed an increased frequency of interactions with the other centromeres. Focusing on the 50kb pericentric region of each chromosome, we found that most CEN-CEN interactions were minimally affected by the loss of chromosome III tDNAs. For instance, interactions between the chromosome XVI centromere and the remaining centromeres showed that interactions between *CEN16* with the majority of centromeres remained unchanged, but that there was a ~20% increase in interaction strength between *CEN16* and *CEN3* when chromosome III lacked tDNAs (Figure 7B).

This increase in *CEN3* interaction was not confined to *CEN16*. When the same analysis was performed using *CEN3* as an anchor, we observed increased frequency of interactions between *CEN3* and all of the other chromosomal centromeres in the tDNA delete strain (Figure 7C). Most of the interaction counts increased approximately 20% compared to WT, with the highest increase seen at C*EN3-CEN9*. The increase in the CEN3-CEN interactions in the tDNA deletion strain was significantly higher ($p=1.22x10^{-14}$) compared to values of all CEN16-CEN interactions (excluding CEN16-CEN3). These results show that upon deletion of all tDNAs across chromosome III, inter-chromosomal

384 interactions increase between *CEN3* and the other centromeres, suggesting that
385 functional tDNAs likely antagonize CEN-CEN associations during interphase.

386 **tDNAs play a role in *HML-HMR* long-range association**

387 The silent loci *HML* and *HMR* reside on chromosome III separated by approximately
388 300kb along the linear chromosome. However, the *HML* locus, located 11kb from
389 *TEL3L*, is in close three-dimensional proximity to the *HMR* locus, located 23kb from
390 *TEL3R*. This long-range interaction has previously been detected using both live-cell
391 microscopy and HiC analysis (Dekker et al., 2002; Kirkland and Kamakaka, 2013; Miele
392 et al., 2009) and we recapitulate this finding in the Micro-C experiment with the wild type
393 strain (Figure 8A). Comparing wild type cells to the tDNA delete strain, we noticed that
394 the interaction of *HML* with *HMR* was slightly altered in the tDNA delete strain. In wild
395 type cells, there was an interaction between *HML* and *HMR* and this interaction zone
396 became less defined and more diffuse upon deletion of the tDNAs and a slightly
397 increased interaction frequency was observed across a broader region of chromosome
398 III. While *HMR* still interacted with *HML* in the deletion strain, it appeared to also display
399 interactions with other loci (including *TEL3L)*. Similarly, the segment containing
400 *HML/TEL3L* showed increased interactions with *TEL3R* rather than being restricted to
401 interacting with sequences at *HMR*. These results suggest that deletion of chromosome
402 III tDNAs subtly perturbed *HML-HMR* long-range interactions.

403 Given that Micro-C measures population averages of stable long-range interactions
404 we decided to measure *HML-HMR* interactions in live cells using fluorescence
405 microscopy. We wished to determine if the tDNA located adjacent to *HMR* influenced
406 *HML-HMR* interactions. We generated a strain with multiple Lac operator sequences

inserted adjacent to *HMR* (at the *GIT1* gene) and multiple copies of the Tet operator sequences inserted adjacent to *HML.* Expression of the fusion proteins CFP-LacI and YFP-TetR in this strain enabled us to visualize these loci in living yeast by fluorescence imaging. The distance between *HML* and *HMR* was then measured in wild type and a strain lacking the t0 tDNA (Figure 8B). We found that in wild type cells, *HML* was in close proximity to *HMR* and the median distance between these loci was 425nm. Consistent with our expectations, deletion of Sir proteins resulted in separation of these loci, with the median distance increasing to 840nm, validating this assay. Importantly, when we eliminated the t0 tDNA, this led to an increase in the distance between *HML* and *HMR* compared to wild type cells, with the median distance between *HML* and *HMR* shifting to 706nm upon deletion of the tDNA. Given the presence of outliers in the data we used a Mann-Whitney U-Test to determine statistical significance between wild type and the various mutants. With an n of approximately 300 cells for the wild type and tDNA delete strain we observed a p value of 3.1 e^{-14} showing that the differences observed were statistically significant. Closer analysis of the plot also indicates that upon deletion of the tDNA there is heterogeneity in the distances between the two loci and there is a continuum of values. Thus there are cells where the two loci are in very close proximity as well as cells where the two loci are very far apart and cells where the loci are at intermediate distances. This might help explain the fact that the difference observed by Micro-C is not large.

The tDNA t0 is necessary for the recruitment of cohesins to the silenced loci and the SMC proteins are necessary for long-range *HML-HMR* interactions (Kirkland and Kamakaka, 2013). However not all tDNAs are equivalent in their ability to recruit

cohesins to the silenced loci (Donze and Kamakaka, 2001; Dubey and Gartenberg, 2007). We therefore inquired if tDNAs that are unable to recruit cohesins are able to restore long-range association between *HML* and *HMR*. We replaced the *HMR* $tDNA^{THR}$ (t0) with $tDNA^{THR}$ (NL1) from chromosome XIV. This tDNA has identical sequence to the t0 tDNA in the body of the gene and therefore has the identical BoxA and BoxB promoter sequence and spacing as tDNA t0. However sequences flanking this tDNA are distinct and the NL1 tDNA is unable to recruit/bind cohesins (Donze and Kamakaka, 2001; Dubey and Gartenberg, 2007). When we replaced a 300bp t0 tDNA-containing fragment with a 300 bp NL1 tDNA-containing fragment we found that the NL1 tDNA was not able to robustly restore long-range *HML-HMR* interactions, suggesting that tDNA mediated cohesin loading might be necessary for these long-range interactions.

Replication fork pausing at tDNA mediates long-range chromosomal interactions

We had previously shown that double strand repair proteins help deposit cohesins to the silenced loci, which then led to homology dependent long-range interactions between *HML* and *HMR* (Kirkland et al., 2015; Kirkland and Kamakaka, 2013). Since we had discovered that a specific tDNA played a role in the clustering of *HML* and *HMR*, we wished to know the mechanism by which this phenomenon occurred. Replication fork pausing/stalling is observed at many tDNAs. This results in the deposition of γ-H2A at the tDNA and this is necessary for fork recovery from the pause/stall (Achar and Foiani, 2017; Azvolinsky et al., 2009; D'Ambrosio et al., 2008; Deshpande and Newlon, 1996; Kirkland and Kamakaka, 2013; Lengronne et al., 2004; Szilard et al., 2010). Rrm3 and topoisomerases play a role in the recovery of stalled replication forks at protein bound

453 sites in the genome such as tDNAs (Achar and Foiani, 2017; Azvolinsky et al., 2006;
454 Ivessa et al., 2003). Therefore we analyzed the effect of these mutants on *HML-HMR*
455 long-range association. The data show that deletion of Rrm3 as well as mutants in the
456 DNA polymerase-ε subunit Dpb3 and the topoisomerase Top1 lead to a statistically
457 significant decrease in *HML-HMR* long-range association (Figure 5B and figure legend).
458 Thus the presence of a tDNA as well as normal Rrm3, Top1 and Dpb3 function are
459 necessary for the establishment or maintenance of the long-range association between
460 *HML* and *HMR*.

461 **tDNA presence enhances epigenetic gene silencing at clustered *HML-HMR***

462 Since the t0 tDNA located adjacent to the silenced *HMR* domain is necessary for the
463 long-range clustering of the silenced domain, we wondered if reduction in clustering had
464 any effect on gene silencing. We asked whether tDNA mediated loss of *HML-HMR*
465 interactions affected gene silencing at *HML* and *HMR*. Silencing can be assayed by
466 insertion of reporter genes within or immediately adjacent to the silenced domains. In
467 wild type yeast when a reporter gene is inserted immediately adjacent to these loci, the
468 genes is metastably silenced. A cassette containing an H2B (*HTB1*) promoter driving
469 *HTB1-EYFP* was integrated to the right of *HML* while a cassette containing the *HTB1*
470 promoter driving *HTB1-ECFP* was integrated to the left of *HMR*. In addition, on
471 chromosome XV, a cassette containing an *HTB1*promoter driving *HTB1*-mCherry was
472 integrated as a control euchromatic marker (Mano et al., 2013). The *HTB1*-mCherry
473 gene is active in all cells in the population. The *HML::YFP* and the *HMR::CFP* reporter
474 genes are present immediately outside of *HML* and *HMR* but reside in a region bound
475 by Sir proteins (Oki and Kamakaka, 2005; Ruben et al., 2011). These genes adopt one

476 of two expression states, either active or silent. For visualization, single cells were
477 placed on microfluidic plates and monitored continuously by fluorescence microscopy.
478 Fluorescent signal from each individual cell was recorded every 40 minutes over a
479 period of ~24 hours. This allowed us to trace the lineage of each daughter from the
480 founder cell and score the cells according to the expression of the reporter genes at
481 *HML* and *HMR*. Cell lineage trees were traced and each cell in the lineage was
482 assigned a positive or negative value for expressing each reporter as it underwent cell
483 division (Figure 9A).

484 We initially analyzed the silencing of the reporter genes in the wild type strain.
485 Consistent with previous data (Mano et al., 2013), reporters at *HML* and *HMR* were
486 regulated such that the reporters maintained their activity state over many generations
487 and occasionally switched to the opposite expression state. Once they switched they
488 maintained the new state for several generations. Furthermore, when one reporter was
489 active the other was also more likely to be active suggesting long-range coordination
490 between *HML* and *HMR* though this coordination is not absolute.

491 We next investigated silencing of the reporters in a strain where chromosome III
492 lacked all the tDNAs. In this strain, the reporter at *HMR* was active more often
493 compared to the wild type strain. While the effect was not as pronounced, the same
494 effect was also observed at *HML* (Figure 9A tDNA delete panel). Furthermore, the
495 silenced state was less stable, and switched to the active state more often. This
496 suggests that silencing at these loci is influenced by the tDNAs.

497 While expression states at both *HML* and *HMR* were stably inherited, the
498 transcriptional state did flip in daughter cells (Figure 9B). An expressed to repressed

transition was a less frequent event compared to the repressed to expressed transitions regardless of genotype. This is not entirely surprising since the reporter genes were inserted immediately outside of the two silencers in a zone where the silent state is metastable (Valenzuela et al., 2008; Valenzuela et al., 2006). However, when analyzing the repressed to expressed transitions, we saw a discernible difference in the frequency of the expression of the reporter genes at *HMR*. The full tDNA delete strain showed an increased frequency of cells undergoing the transitions at *HMR* compared to wild type cells and the inverse was seen for the expressed to repressed transition (Suppl. Table 3).

Taken together, the data suggest that deletion of tDNAs on chromosome III had an effect on the ability of *HMR* to interact with *HML* and diminution of this clustering led to an alteration in the stability of the silenced state at these loci.

Discussion

tDNAs are middle repetitive DNA sequences scattered across all 16 chromosomes and their primary function is the synthesis of tRNAs. In this manuscript, we show that tDNAs affect local chromatin structure, which then impinges on chromosome architecture. tDNAs 1) affect chromatin structure by maintaining local nucleosome free regions along the fiber and precisely positioned nucleosomes immediately outside of the tDNAs, 2) recruit cohesins and condensins 3) affect nuclear architecture by influencing centromere clustering and 4) alter heterochromatin clustering leading to changes in the fidelity of inheritance of gene silencing.

The binding of specific proteins such as CTCF to a site on the DNA can affect nucleosome positions over long distances (Fu et al., 2008). Nucleosome depletion at the gene and positioned nucleosomes flanking the gene is a hallmark of tDNAs (Cole et al., 2012; Dhillon et al., 2009; Dion et al., 2007; Harismendy et al., 2003; Moqtaderi and Struhl, 2004; Nagarajavel et al., 2013; Oki and Kamakaka, 2005; Roberts et al., 2003; Yuan et al., 2005). Our data show that loss of the tDNA promoters' only affect nucleosome positions in the immediate vicinity of the tDNA. The nucleosome positioning effects mediated by the tDNA bound transcription factors TFIIIC and TFIIIB are not transmitted over long distances.

tDNAs, SMC proteins and chromatin folding

The SMC proteins are involved in higher order chromosome organization in all eukaryotes and have been extensively mapped. tDNAs are binding sites for all three classes of SMC proteins (cohesin, condensin and repairsin), the SMC protein loaders Scc2 and Scc4 and the meiotic Rec8 SMC protein (Blat and Kleckner, 1999;

538 D'Ambrosio et al., 2008; Glynn et al., 2004; Klein et al., 1999; Kogut et al., 2009;
539 Laloraya et al., 2000; Lindroos et al., 2006; Noma, 2017). Given these intimate
540 connections between tDNAs and the SMC proteins our data indicate that loss of the
541 tDNA promoters does lead to loss of SMC proteins from tDNAs but this effect is tDNA
542 specific since we do not see a loss of SMC proteins from centromeres or Scc2 from
543 other sites in the genome. Surprisingly the loss of Scc2 and Brn1 from tDNAs does not
544 affect chromatin folding. While clustering of tDNAs in the nucleus (as measured by
545 fluorescence microscopy) is dependent upon the SMC proteins (Haeusler and Engelke,
546 2006; Noma et al., 2006) the precise contribution of tDNAs in this process remained
547 unclear. Our Micro-C analysis of chromosome III suggests that tDNAs are unlikely to be
548 the key drivers of chromatin looping and folding or tethering to nuclear substructures
549 since we did not observe any change in contact frequency across the entire
550 chromosome. Furthermore, we did not observe any discernible effect on chromosome
551 loss rates or chromosome mobility. It is likely that tDNA independent SMC protein
552 binding sites masks the tDNA-mediated effects. SMC proteins bind only half of the
553 tDNAs in the nucleus and only a third of the SMC protein binding sites localize at or
554 near tDNAs (D'Ambrosio et al., 2008). The lack of phenotype would also be consistent
555 with previous data that showed that a reduction in the levels of the SMC proteins does
556 not affect the properties of the chromosome arm (Heidinger-Pauli et al., 2010). Recently
557 a synthetic yeast chromosome III was generated and characterized (Annaluru et al.,
558 2014; Mercy et al., 2017). The synthetic chromosome lacks repetitive sequences such
559 as TY elements, LTRs and tRNA genes. The 3D structure of this chromosome was
560 determined using HiC and the data show that there were no major differences between

this chromosome and the wild type chromosome except for a shortening of the length. While this chromosome lacks multiple elements the three-dimensional folding data are consistent with our conclusions from the Micro-C analysis of the same chromosome lacking only tDNAs. While it is possible that redundancy of structural elements masks tDNA-mediated effects on chromatin folding it is also possible that chromatin folding is driven by underlying DNA sequence and not tDNA mediated interactions. The yeast chromosomes have isochores with G-C rich, gene rich R-band segments alternating with AT-rich G-band segments (Dujon, 1996; Sharp and Lloyd, 1993), which exhibit different functional properties (Blat et al., 2002; Dekker, 2007). Chromosome III has a G-C segment from 20 to 100 kb on the left arm followed by an A-T rich central segment from 100 to 200kb on the right arm and then a second G-C rich segment from 200 to 290kb on the same arm. In this scenario, the underlying A-T rich DNA sequence likely plays a dominant role in the three dimensional folding of chromatin. tDNAs are often syntenic along chromosomes (Raab et al., 2012; Raab and Kamakaka, 2010) and it is possible that these positions have been selected for optimal gene activity rather than being involved in chromatin loop formation (Gehlen et al., 2012). Thus while the A-T rich isochore is structurally and functionally distinct (Baudat and Nicolas, 1997; Dekker et al., 2002; Gerton et al., 2000) and is the region rich in tDNAs (See Figure1) our results would suggest that the tDNAs do not play a significant role in either tethering of this isochore or the overall folding of this segment. The tDNA clustering observed by microscopy could simply be a function of linear proximity of tDNAs along the chromatin fiber.

tDNAs and centromere clustering

584 Chromosome tethering to nuclear substructures enables nuclear organization
585 (Gehlen et al., 2012; Taddei et al., 2010) and centromeres and the telomeres along with
586 their associated proteins play a key role in this process (Andrulis et al., 2002; Bupp et
587 al., 2007; Bystricky et al., 2004; Duan et al., 2010; Gartenberg et al., 2004; Guacci et
588 al., 1997; Jin et al., 2000; Mekhail et al., 2008; Schober et al., 2009; Taddei and Gasser,
589 2004; Tjong et al., 2012). All sixteen centromeres cluster together in a ring around the
590 membrane-embedded spindle pole body. The centromeres are tethered to the spindle
591 pole body via direct interactions between kinetochore-associated proteins and the
592 spindle pole body associated microtubules in interphase (Bystricky et al., 2004; Dekker
593 et al., 2002; Guacci et al., 1997; Jin et al., 2000). Other factors are likely to influence
594 this phenomenon but remain unknown. tDNA density is almost 2 fold higher in the
595 pericentric region of *S. cerevisiae* chromosomes including chromosome III (Snider et al.,
596 2014) (see Figure 1). While tDNAs have been shown to help tether centromeres to the
597 spindle axis during mitosis (Snider et al., 2014), in interphase nuclei, the loss of tDNAs
598 results in increased interactions between the clustered centromeres. The physical
599 presence of tDNAs in the pericentric region could interfere with the close packaging of
600 centromeres during interphase. This could be due to transcription-mediated effects
601 since tRNA genes are highly active. In *S. pombe,* mutations that reduce tDNA
602 transcription result in increased tDNA association with the centromere and increase
603 chromosome condensation during mitosis. Furthermore, tDNA association with
604 centromeres increases when the genes become inactive (Iwasaki et al., 2010). Thus,
605 tDNA clustering at transcriptionally active RNA pol III transcription factories near the
606 centromeres could hinder closer centromere-centromere interactions during interphase

while a decrease in tDNA transcription during mitosis could help tether centromeres to the spindle axis during mitosis (Snider et al., 2014).

An alternative though not mutually exclusive possibility is based on the observation that transcriptionally active tDNAs interact with nuclear pores (Casolari et al., 2004; Chen and Gartenberg, 2014; Ruben et al., 2011). It is thus possible that there is a competition between pericentric tDNA- nuclear pore interactions in opposition to centromere-centromere interactions. In this scenario, the loss of tDNA tethering to the nuclear pore would enable the centromere greater freedom of movement thus enabling closer centromere-centromere interactions.

tDNA effects on *HML-HMR* interactions and the inheritance of gene silencing

Gene silencing is primarily a function of the Sir proteins though numerous other factors influence the process (Gartenberg and Smith, 2016). Proto-silencers are sequence elements that on their own are unable to silence a gene, but when located near a silencer increase the efficiency of silencing (Fourel et al., 2002; Lebrun et al., 2001). Our demonstration that the tDNA affects silencing of a reporter adjacent to the silent *HMR* domain suggest that tDNAs function as proto-silencers. Our data suggest that tDNA mediated clustering of silent loci might be important in the silencing of these loci and the loss of long-range association might reduce the efficient inheritance of the silent state. This is analogous to the observations that gene clustering at active chromatin hubs and transcription factories increases the efficiency of transcription as well as the data showing that telomere clustering increases the efficiency of silencing at sub-telomeric sequences (Gasser et al., 2004).

629 This unexpected observation also raises the question of how might tDNAs influence
630 long-range *HML-HMR* interactions. tDNAs, including the tDNA next to *HMR,* are sites of
631 replication slowing/pausing (Admire et al., 2006; Azvolinsky et al., 2009; Deshpande
632 and Newlon, 1996; Ivessa et al., 2003; Lemoine et al., 2005; Wang et al., 2001). The
633 tDNA adjacent to *HMR* is a site of replication fork pausing (Kitada et al., 2011; Szilard et
634 al., 2010). We recently showed that long-range *HML-HMR* interactions require
635 homologous sequences to be present at these loci (Kirkland et al., 2015; Kirkland and
636 Kamakaka, 2013) and we now show that mutations in replication coupled homologous
637 recombination repair proteins including the SMC proteins, Rrm3, Top1 and Dpb3 lead to
638 a reduction in *HML-HMR* interactions. Based on the accumulated data we would posit
639 that replication fork slowing/pausing results in the deposition of γH2A and SMC proteins
640 at tDNAs followed by a homology search leading to *HML-HMR* interactions. The re-
641 formation of silenced chromatin following replication precludes the eviction of γH2A
642 (Keogh et al., 2006) thereby stabilizing SMC protein binding, which then maintains the
643 long-range *HML-HMR* association. The tDNAs thus help initiate a network of
644 interactions mediated by the SMC proteins and the Sir proteins leading to *HML-HMR*
645 association and chromosome folding. We would like to posit that a series of transient
646 interactions during replication aid in the setting up of the final optimal nuclear
647 architecture found in the interphase nucleus.

648 In conclusion, tDNAs primarily affect local chromatin structure. Each tDNA affects
649 nucleosome positions and protein binding in its immediate vicinity. These local
650 perturbations functionally and structurally interact with neighboring regulatory regions
651 resulting in tDNA mediated pleiotropic effects. In some instances tDNAs affect the

652 expression of neighboring pol II transcribed genes by the phenomenon of local tgm
653 silencing. In another context tDNA mediated replication pausing result in the
654 establishment of long-range heterochromatin interactions, which then influence the
655 inheritance of silencing states at these loci.
656

657 **Acknowledgements**

658 This work was supported in part by a grant from the NIH to RTK (GM078068) and (T32-
659 GM008646) to JK, OH and KW. This study was funded in part by the Intramural
660 Research Program of the National Institutes of Health (NICHD). We thank the NHLBI
661 Core Facility for paired-end sequencing of the micrococcal nuclease libraries. The
662 Functional Genomics Laboratory, UC Berkeley sequenced the ChIP-Seq libraries on an
663 Illumina HiSeq4000 at the Vincent J Coates Laboratory at UC Berkeley, supported by
664 an NIH S10 OD018174 Instrumentation Grant.
665

Materials and Methods

Yeast strains and primers

Table S1 and S2 list the yeast strains and the primer sequences that were used in this study.

MNase-Seq

MNase-Seq experiments were carried out as previously described (Cole et al., 2012). In brief, isolated nuclei were digested with MNase to mono-nucleosomes. Paired-end sequencing libraries were prepared (Illumina). Paired reads (50 nt) were mapped to the reference genome (SacCer2) using Bowtie-2 (Cole et al., 2014; Langmead and Salzberg, 2012; Ocampo et al., 2016). For analysis of nucleosome occupancy (coverage) at tDNAs, both across the genome and on chromosome III, tDNAs were aligned on their start sites or at the deletion points. Data sets were normalized to their genomic average, set at 1, using only DNA fragments in the 120 to 180 bp range. In one experiment, mono-nucleosomal DNA was gel-purified, but not in the replicate, in which short fragments (< 120 bp) derived from digestion of the TFIIIB-TFIIIC complex at tDNAs (Nagarajavel 2013) were observed. The MNase-seq data are available at the GEO database:(GSE98304 https://www.ncbi.nlm.nih.gov/geo/query/acc.cgi?token=wnynwaoqvnktfmb&acc=GSE98304)

ChIP-Seq and RNA-Seq

Chromatin immunoprecipitation reactions were performed essentially as described above but elution of the precipitated DNA from Protein A/G beads was carried out with two successive washes in 175ul of 0.1M $NaHCO_3$/1% SDS. 50ul of each input sample

689 was diluted to 350ul with the elution buffer. NaCl was added to a final concentration of
690 0.2M and cross-links were reversed with an overnight incubation at 65C in a
691 Thermomixer. All samples were treated with 60ug of RNAase A (Sigma) at 37C for 60'
692 followed by a Proteinase K (Roche) treatment at 50C for 60'. DNA was purified with a
693 successive phenol chloroform and chloroform extraction followed by precipitation with 2
694 volumes of ethanol and 50ug of glycogen (Roche).
695 The ChIP and Input DNA was spun, washed with 70% ethanol and re-suspended in
696 deionized water. DNA quantitation was performed using a Qubit dsDNA HS Assay kit
697 prior to confirmation by qPCR.
698 Libraries for ChIP-Seq were prepared at the Functional Genomics Laboratory, UC
699 Berkeley and sequenced on an Illumina HiSeq4000 at the Vincent J Coates Laboratory
700 at UC Berkeley.
701 For RNA-Seq, yeast strains JRY2334 and JKY690 were grown in duplicate in 50ml YPD
702 to a cell density of 6-7x10^6 cells/ml, spun, washed in 25ml PBS, divided into 4 aliquots
703 per culture and transferred to 1.5ml microfuge tubes. Cell pellets were flash frozen in
704 liquid N2 and transferred to -70C. RNA, library preparation and sequencing for RNA-
705 Seq were performed by ACGT Inc. Wheeling, IL.
706 Transcript abundances were estimated using Kallisto (Bray et al., 2016). Differential
707 analysis of gene expression data was performed using the R package Sleuth (Pimentel
708 et al., 2017). Likelihood ratio test and Wald test were used to identify the differentially
709 expressed genes (false discovery rate adjusted p-value (or q-value) < 0.05 in both
710 tests). Since the likelihood ratio test does not produce any metric equivalent to the fold

711 change, we used the Wald test to generates the beta statistic, which approximates to
712 the log2 fold change in expression between the two conditions.
713 Sequence data have ben deposited in the GEO database.
714 https://www.ncbi.nlm.nih.gov/geo/query/acc.cgi?token=krihsykczdmbpox&acc=GSE106
715 250
716 **ChIP**
717 ChIP-qPCR experiments on all Brn1 and Scc2/4 were performed as previously
718 described (Dhillon et al., 2009; Kirkland and Kamakaka, 2013). In brief, yeast cells of a
719 strain of interest were inoculated and grown overnight in 300 ml of YPD media to an OD
720 of 1-2. These cells were then fixed in 1% formaldehyde for a duration of 2 hours at
721 room temperature. The reaction was then quenched with glycine, and the cells were
722 spun down and washed in 1X PBS. The cross linked cells were then flash frozen in dry
723 ice and stored at -70^{0}C. In preparation for IP, the cells were thawed on ice, broken
724 apart by bead beating, and sonicated to achieve a desired chromatin size of ~300 bp.
725 Once the size of the chromatin was checked, cell debris was cleared from the sample
726 by high-speed centrifugation. The cross linked, sized chromatin was split into 2
727 samples and IP's were done overnight in the presence of both an antibody to the protein
728 of interest as well as pre-blocked A/G-Sepharose beads at 4^{o}C. 50 µl of input
729 chromatin was also taken from each IP sample prior to addition of the antibody.
730 Chromatin elution was done using 10% Chelex 100 (Bio-Rad) along with proteinase K
731 treatment. After elution, both input and IP DNA were quantitated via a Picogreen
732 fluorescent quantification assay (Invitrogen). For each qPCR reaction, input DNA was
733 run in triplicate and IP DNA was run in duplicate. An equal amount of input and IP DNA

was used in each individual reaction. The enrichment for a given probe was then calculated as IP/Input, and was further normalized to the OCA4 locus. The results of each ChIP-qPCR are comprised from two independent crosslinks per strain assayed, and for each crosslink two independent IPs were done.

Mean Squared Distance Analysis

Mean-squared distance analysis was carried out as previously described (Hediger et al., 2002; Heun et al., 2001; Verdaasdonk et al., 2013). In brief, we built strains that contained a 64x lacO array at specific points along chromosome III. We then integrated a cassette containing an spc29-RFP fusion protein elsewhere in the genome. This protein is an essential kinetochore protein, and therefore serves as a marker for the spindle pole body. The spindle pole body served as a fixed point to which we could measure the movement of our GFP tagged loci in 3D space over a period of 10 minutes. Z-stack images of the cells were taken every 30 seconds during the time-lapse, and the data are used to calculate the radius of constraint using the equation: $\langle (X_t - X_{t+\Delta t})^2 \rangle$. MSD curves were generated for each locus in both the WT and tDNA delete strain (Supplementary Figure 2). The plateau of the MSD curve was used to calculate the radius of constraint (Rc) for each locus. This analysis was performed in no less than 35 cells per genotype assayed. The data were plotted in “NotBoxPlots” (source code obtained from https://github.com/raacampbell/notBoxPlot)

***HML-HMR* Colocalization analysis**

Distance assays between *HML* and *HMR* was performed as previously described (Kirkland and Kamakaka, 2013). Fluorescence microscopy was performed on live yeast cells after growing the cells in YMD with Leucine, uracil, tryptophan, lysine, adenine and

757 histidine. Cells were grown to an Od A600 of approximately 0.6. Cells were washed in
758 YMD, placed on YMD-agar patches on slides, and imaged. Microscopy was performed
759 using an Olympus xi70 inverted wide-field microscope with DeltaVision precision stage
760 using a Coolsnap HQ2 camera and a 100x/1.4 oil objective. The 20 image stacks for
761 each image were acquired with a step size of 200nm using the appropriate wavelength
762 for CFP, YFP, GFP or mCherry. The acquisition software used was softWoRx3.7.1. The
763 images were cropped using Adobe Photoshop. For the distance analysis between *HML*
764 and *HMR*, the distance between the yellow and cyan dots were calculated in
765 nanometers using the “measure” tool in three dimensions. The measured distances
766 were loaded into R software (www.r-project.org) and the data were plotted as a box plot.
767 The box includes the middle 50% of the data with the line in the box being the median
768 value. The data presented are the sum of at least two independent strains.

769 **Single Cell Expression Analysis**

770 Single cell expression analysis was performed as previously described (Mano et al.,
771 2013). Briefly, cells were grown in YPD at 30C and placed in a microfluidics device.
772 Time-lapse photos of growing cells were recorded using an Axio Observer Z1
773 microscope using a 40x objective. The ECYP and EYFP fluorescence intensities were
774 normalized to the highest level of fluorescence observed and the Euchromatic mCherry
775 signal.

776 **Micro-C**

777 Micro-C was performed as previously described (Hsieh et al., 2015). The detailed
778 method have been described (Hsieh et al., 2016). In brief, this technique provides
779 nucleosome level resolution of all of the interactions occurring across the genome by

using MNase digestion in lieu of a restriction enzyme as in traditional Hi-C techniques. The interactome data were deposited in the GEO database GSE98543 (https://www.ncbi.nlm.nih.gov/geo/query/acc.cgi?acc=GSE98543)

Antibodies

Antibodies used in ChIP were as follows; Scc2-Myc: anti-myc 9E10 (Abcam) = 5 µl, Brn1-HA: anti-HA HA.11 (Covance) = 5 µl.

Figure Legends:

Figure 1) Schematic of Budding Yeast Chromosome III

The positions of the 10 tDNAs on chromosome III are shown. Yellow arrowheads denote tDNAs and the direction of the arrowhead indicates the direction of transcription. Blue arrowheads mark other loci of interest in this study.

Figure 2) Deletion of tDNAs leads to local changes in chromatin structure

Left Panel: Comparison of nucleosome occupancy at 265 tDNAs on all of yeast chromosomes except chromosome III. The tDNAs were aligned on their transcription start sites (TSS set at 0). WT (black) tDNA delete (red).

Right Panel: Analysis of the nucleosome occupancy at tDNAs on chromosome III in the wild type and tDNA delete strain.

Figure 3) Scc2 binding along chromosome III in the wild type and tDNA delete strain

ChIP-seq mapping of Myc-Scc2. The top panels show the distribution of Scc2 at tDNAs on chromosome III in wild type cells (left) and tDNA delete strains (right). Bottom panels show the distribution of Scc2 at 265 tDNAs on all chromosomes except chromosome III in the wild type (left) and the tDNA delete strain (right).

Figure 4) Scc2 and Brn1 binding at tDNAs on chromosome III

A) ChIP-qPCR mapping of Myc-Scc2. The data show the distribution of Scc2 at specific sites along chromosome III in the wild type and tDNA delete strain. The data

808 are the results of two independent crosslinks from which four IP's were performed. For
809 each amplicon, the fold enrichment compared to input was first calculated and the data
810 were then normalized to the *OCA4* locus. An unpaired t-test assuming unequal SD was
811 used to test for significance of differences between the wild type and tDNA delete strain.

812 B) ChIP-qPCR mapping of HA-Brn1, condensin. Fold enrichment and statistical
813 significance was calculated in the same way as for the Scc2 ChIP and normalized to the
814 *OCA4* locus.

815 **Figure 5) Effect of tDNA deletion on chromosome III mobility**

816 Mean square displacement analysis of seven loci along chromosome III in wild type
817 and tDNA delete strains are shown. Box plots represent the data obtained from the
818 MSD experiments. Components of the boxplot are as follows; red line represents the
819 mean, pink bar is the 95% confidence interval, purple bar is the standard deviation, and
820 the grey dots represent individual values obtained from each cell analyzed. The green
821 arrowheads beneath the chromosome III schematic show the locations of the loci
822 assayed. The radius of constraint (Rc) measurement was calculated from MSD graphs
823 that were generated over the course of a 10-minute time-lapse movie. These
824 experiments are the result of time-lapse images taken from at least 35 cells per locus
825 assayed. A t-test was used to determine significance of differences observed between
826 the wild type and tDNA delete strain for each loci.

827 **Figure 6) Micro-C Interaction plots of chromosome III.**

828 The heat maps show the interactomes for both wild type and tDNA delete strains for

chromosome III. The X and Y-axes show the positions along the chromosome. Areas of red denote regions of high densities of internucleosomal interactions, while lighter colored areas denote decreased interaction.

Figure 7) Micro-C analysis of the centromeres

A) Deletion of tDNAs on chromosome III leads to an increase in *CEN3* interaction with all other centromeres in the genome. Micro-C experiment analysis of *CEN-CEN* interactions is shown. The heat maps show a piled alignment of all centromeres. Interaction frequencies are denoted by the colored bar to the right of each heat map.

B) The graphs are a quantification of *CEN-CEN* interactions. The graph examines the interaction of *CEN16* with all other centromeres. The x-axis is the interaction counts of a 50 kb segment centered on each centromere (in parts per million).

C) The graph examines the interaction of *CEN3* with all other centromeres. The x-axis is the interaction counts of a 50 kb segment centered on each centromere (in parts per million). The increase in the CEN3-CEN interactions in the tDNA deletion strain was significantly higher ($p=1.22x10^{-14}$) compared to values of all CEN16-CEN interactions (excluding CEN16-CEN3).

Figure 8) Long-Range *HML-HMR* association

A) Deletion of tDNAs on chromosome III leads to a change in *HML-HMR* interaction as measured by Micro-C. Heat maps display the interaction profile between segments on chromosome III that include *HML* and *HMR* (obtained from the Micro-C data). Increased interactions are denoted by red and decreased interactions are denoted by

850 blue. The data are displayed in a log2 format. The x and y axes denote the area of the
851 chromosome displayed on each axis of the heat map.

852 B) Deletion of tDNA t0 leads to perturbation of *HML-HMR* long-range association.
853 The violin plots show data of the distances between *HML*::TetR-YFP and *HMR*::CFP-
854 LacI foci in asynchronously growing strains. Mann-Whitney U-Test were performed to
855 determine statistical significance between wild type and the various mutants. Wild type
856 (n=305), *sir4*Δ (n=134) (p=6.7 e^{-16}), tDNA t0Δ (n=317) (p=3.1 e^{-14}) or t0Δ:NL1 (n=330)
857 (p=2.2 e-^{16}) strains. The dark line in the middle represents the median distance. The
858 data for *sir4Δ* are shown as a control and are the same as those in (Kirkland and
859 Kamakaka, 2013).

860 C) Replication–repair proteins are necessary for *HML-HMR* interactions:
861 Violin plots of the distance between TetR-YFP and CFP-LacI foci in a given wild type
862 or mutant strain are shown. rrm3Δ (n=208) (p=4.8 e^{-12}), dpb3Δ (n=134) (p=1.7 e^{-10})
863 top1Δ (n=139) (p=4.2 e^{-12}) scc2D730V (n=188) (p=1.9 e^{-14}). The data for the
864 *scc2D730V* allele are simply shown as a control and are the same as those in (Kirkland
865 and Kamakaka, 2013).

866 **Figure 9) Silencing of reporter genes at *HML* and *HMR***

867 A) tDNAs on chromosome III modulate silencing of reporter genes at *HML and HMR*.
868 Representative lineage trees of the different strains that were analyzed are shown. Wild
869 type refers to a strain containing all tDNAs on chromosome III. tDNA delete refers to a
870 strain lacking any tDNAs on chromosome III. The expression of *HML::EYFP* or
871 *HMR::ECFP* in each generation of cells was monitored, quantitated and is indicated by

the presence of their respective colors in the cells of the tree.

B) Deletion of tDNAs on chromosome III leads to a change in the maintenance of silencing at *HML* and *HMR*. The graphs quantify the changes in expression state of *HML::EYFP* and *HMR::ECFP* between generations in the different genotypes studied. Expressed to repressed transitions identify reporters that were expressed in one generation but not expressed in the next. Repressed to expressed transitions represent reporter genes that were not expressed in one generation but expressed in the next.

Table1

Genes whose mRNA levels changed in the tDNA delete strain compared to the wild type along with statistical analysis of the differences in expression levels.

Supplementary Figure 1) Nucleosome occupancy plots at five tDNA deletion points on chromosome III. MNase-seq data for wild type and tDNA delete were normalized to the genomic average (= 1). Coverage plots are shown using all DNA fragments in the 120 to 180 bp range. The reference point (0) is the nucleotide marking the 5'-end of the deletion on chromosome III. Upstream of the deletion point at 0, the DNA sequence is the same in wild type and the tDNA delete chromosome III. Downstream of the deletion point, the DNA sequences are different. The black arrow shows the location and orientation of the tDNA in wild type chromosome III. Meaningful plots cannot be made for two tDNAs (tP(AGG)C and tS(CGA)C), because they were moved to another chromosome. Two other tDNAs (tM(CAU)C and tK(CUU)C) are present in S288C strains but are naturally absent in W-303 strains, including the strains used here. The wild type profile is in orange and the tDNA delete profile is in blue.

Supplementary Figure 2) Deletion of tDNAs does not lead to general changes in chromatin structure at RNA pol II transcribed genes on chromosome III. Comparison of global nucleosome phasing on chromosome III in wild type (blue line) and tDNA delete (red line) cells: average nucleosome dyad positions on 106 RNA Pol II-transcribed genes on chromosome III. These genes cover most of chromosome III. The genes were aligned on their transcription start sites (TSS set at 0). The average nucleosome dyad density is set at 1.

Supplementary Figure 3) ChIP-Seq graphs showing the distribution of Scc2 at specific sites along chromosome III. tDNAs are marked by arrowheads. Graph 1 and 2 are independent ChIP-Seq data from the wild type strain. Graphs 3 and 4 are independent ChIP-Seq data from the tDNA delete strain.

Supplementary Figure 4) Summary graphs for MSD analysis for each genotype The graphs summarize the results of MSD time-lapse experiments for the 8 loci assayed. Both WT (blue) and tDNA delete (red) are shown on each graph. Time-lapse images were taken over a 10 minute period, z-stack images were taken every 30 seconds in 200 nm increments. The distance between the GFP marked locus of interest and spc29-RFP spindle pole body protein was calculated at each 30-second interval. Mean distance traveled for each time-point was used to create the MSD curves. At least 35 cells were assayed for each genotype.

Supplementary Figure 5) Whole genome interaction plots for Micro-C experiments that were done in this study. The heat maps show full genome interactomes for both wild type and tDNA delete strains. On the x-axis, the

916 chromosomes are displayed from chr I to chr XVI going from left to right. On the y-axis,
917 the chromosomes are displayed from chr I to chr XVI going from top to bottom. Areas
918 of red denote increased interaction, while lighter colored areas denote decreased
919 interaction.

920 **Supplementary Table1:** Strain list with genotypes

921 **Supplementary Table2:** Sequences of PCR primers used in this study

922 **Supplementary Table3:** Statistical analysis of differences in expression of
923 *HML::EYFP* and *HMR::ECFP* in the wild type and tDNA delete strains.

924

925

926

927

928

929

930

931 **References**

932

933

934 Achar, Y.J., and Foiani, M. (2017). Coordinating Replication with Transcription. Adv Exp
935 Med Biol *1042*, 455-487.
936 Admire, A., Shanks, L., Danzl, N., Wang, M., Weier, U., Stevens, W., Hunt, E., and
937 Weinert, T. (2006). Cycles of chromosome instability are associated with a fragile site
938 and are increased by defects in DNA replication and checkpoint controls in yeast.
939 Genes Dev *20*, 159-173.
940 Albert, B., Mathon, J., Shukla, A., Saad, H., Normand, C., Leger-Silvestre, I., Villa, D.,
941 Kamgoue, A., Mozziconacci, J., Wong, H.*, et al.* (2013). Systematic characterization of
942 the conformation and dynamics of budding yeast chromosome XII. J Cell Biol *202*, 201-
943 210.
944 Andrulis, E.D., Zappulla, D.C., Ansari, A., Perrod, S., Laiosa, C.V., Gartenberg, M.R.,
945 and Sternglanz, R. (2002). Esc1, a nuclear periphery protein required for Sir4-based
946 plasmid anchoring and partitioning. Mol Cell Biol *22*, 8292-8301.
947 Annaluru, N., Muller, H., Mitchell, L.A., Ramalingam, S., Stracquadanio, G., Richardson,
948 S.M., Dymond, J.S., Kuang, Z., Scheifele, L.Z., Cooper, E.M.*, et al.* (2014). Total
949 synthesis of a functional designer eukaryotic chromosome. Science *344*, 55-58.
950 Azvolinsky, A., Dunaway, S., Torres, J.Z., Bessler, J.B., and Zakian, V.A. (2006). The S.
951 cerevisiae Rrm3p DNA helicase moves with the replication fork and affects replication of
952 all yeast chromosomes. Genes Dev *20*, 3104-3116.
953 Azvolinsky, A., Giresi, P.G., Lieb, J.D., and Zakian, V.A. (2009). Highly transcribed RNA
954 polymerase II genes are impediments to replication fork progression in Saccharomyces
955 cerevisiae. Mol Cell *34*, 722-734.
956 Baudat, F., and Nicolas, A. (1997). Clustering of meiotic double-strand breaks on yeast
957 chromosome III. Proc Natl Acad Sci U S A *94*, 5213-5218.
958 Bausch, C., Noone, S., Henry, J.M., Gaudenz, K., Sanderson, B., Seidel, C., and
959 Gerton, J.L. (2007). Transcription alters chromosomal locations of cohesin in
960 Saccharomyces cerevisiae. Mol Cell Biol *27*, 8522-8532.
961 Biswas, M., Maqani, N., Rai, R., Kumaran, S.P., Iyer, K.R., Sendinc, E., Smith, J.S., and
962 Laloraya, S. (2009). Limiting the extent of the RDN1 heterochromatin domain by a
963 silencing barrier and Sir2 protein levels in Saccharomyces cerevisiae. Mol Cell Biol *29*,
964 2889-2898.
965 Blat, Y., and Kleckner, N. (1999). Cohesins bind to preferential sites along yeast
966 chromosome III, with differential regulation along arms versus the centric region. Cell
967 *98*, 249-259.
968 Blat, Y., Protacio, R.U., Hunter, N., and Kleckner, N. (2002). Physical and functional
969 interactions among basic chromosome organizational features govern early steps of
970 meiotic chiasma formation. Cell *111*, 791-802.
971 Bloom-Ackermann, Z., Navon, S., Gingold, H., Towers, R., Pilpel, Y., and Dahan, O.
972 (2014). A comprehensive tRNA deletion library unravels the genetic architecture of the
973 tRNA pool. PLoS Genet *10*, e1004084.

974 Bray, N.L., Pimentel, H., Melsted, P., and Pachter, L. (2016). Near-optimal probabilistic
975 RNA-seq quantification. Nat Biotechnol *34*, 525-527.
976 Bupp, J.M., Martin, A.E., Stensrud, E.S., and Jaspersen, S.L. (2007). Telomere
977 anchoring at the nuclear periphery requires the budding yeast Sad1-UNC-84 domain
978 protein Mps3. J Cell Biol *179*, 845-854.
979 Bystricky, K., Heun, P., Gehlen, L., Langowski, J., and Gasser, S.M. (2004). Long-range
980 compaction and flexibility of interphase chromatin in budding yeast analyzed by high-
981 resolution imaging techniques. Proc Natl Acad Sci U S A *101*, 16495-16500.
982 Casolari, J.M., Brown, C.R., Komili, S., West, J., Hieronymus, H., and Silver, P.A.
983 (2004). Genome-wide localization of the nuclear transport machinery couples
984 transcriptional status and nuclear organization. Cell *117*, 427-439.
985 Chen, M., and Gartenberg, M.R. (2014). Coordination of tRNA transcription with export
986 at nuclear pore complexes in budding yeast. Genes Dev *28*, 959-970.
987 Chereji, R.V., Ocampo, J., and Clark, D.J. (2017). MNase-Sensitive Complexes in
988 Yeast: Nucleosomes and Non-histone Barriers. Mol Cell *65*, 565-577 e563.
989 Cole, H.A., Howard, B.H., and Clark, D.J. (2012). Genome-wide mapping of
990 nucleosomes in yeast using paired-end sequencing. Methods Enzymol *513*, 145-168.
991 Cole, H.A., Ocampo, J., Iben, J.R., Chereji, R.V., and Clark, D.J. (2014). Heavy
992 transcription of yeast genes correlates with differential loss of histone H2B relative to H4
993 and queued RNA polymerases. Nucleic Acids Res *42*, 12512-12522.
994 D'Ambrosio, C., Schmidt, C.K., Katou, Y., Kelly, G., Itoh, T., Shirahige, K., and
995 Uhlmann, F. (2008). Identification of cis-acting sites for condensin loading onto budding
996 yeast chromosomes. Genes Dev *22*, 2215-2227.
997 Damelin, M., Simon, I., Moy, T.I., Wilson, B., Komili, S., Tempst, P., Roth, F.P., Young,
998 R.A., Cairns, B.R., and Silver, P.A. (2002). The genome-wide localization of Rsc9, a
999 component of the RSC chromatin-remodeling complex, changes in response to stress.
1000 Mol Cell *9*, 563-573.
1001 Dekker, J. (2007). GC- and AT-rich chromatin domains differ in conformation and
1002 histone modification status and are differentially modulated by Rpd3p. Genome Biol *8*,
1003 R116.
1004 Dekker, J., Rippe, K., Dekker, M., and Kleckner, N. (2002). Capturing chromosome
1005 conformation. Science *295*, 1306-1311.
1006 Deshpande, A.M., and Newlon, C.S. (1996). DNA replication fork pause sites
1007 dependent on transcription. Science *272*, 1030-1033.
1008 Dhillon, N., Raab, J., Guzzo, J., Szyjka, S.J., Gangadharan, S., Aparicio, O.M.,
1009 Andrews, B., and Kamakaka, R.T. (2009). DNA polymerase epsilon, acetylases and
1010 remodellers cooperate to form a specialized chromatin structure at a tRNA insulator.
1011 Embo J *28*, 2583-2600.
1012 Dieci, G., Fiorino, G., Castelnuovo, M., Teichmann, M., and Pagano, A. (2007). The
1013 expanding RNA polymerase III transcriptome. Trends Genet.
1014 Dion, M.F., Kaplan, T., Kim, M., Buratowski, S., Friedman, N., and Rando, O.J. (2007).
1015 Dynamics of replication-independent histone turnover in budding yeast. Science *315*,
1016 1405-1408.
1017 Dion, V., Kalck, V., Horigome, C., Towbin, B.D., and Gasser, S.M. (2012). Increased
1018 mobility of double-strand breaks requires Mec1, Rad9 and the homologous
1019 recombination machinery. Nat Cell Biol.

1020 Dixon, J.R., Selvaraj, S., Yue, F., Kim, A., Li, Y., Shen, Y., Hu, M., Liu, J.S., and Ren, B.
1021 (2012). Topological domains in mammalian genomes identified by analysis of chromatin
1022 interactions. Nature *485*, 376-380.
1023 Donze, D., Adams, C.R., Rine, J., and Kamakaka, R.T. (1999). The boundaries of the
1024 silenced HMR domain in Saccharomyces cerevisiae. Genes Dev *13*, 698-708.
1025 Donze, D., and Kamakaka, R.T. (2001). RNA polymerase III and RNA polymerase II
1026 promoter complexes are heterochromatin barriers in Saccharomyces cerevisiae. Embo
1027 J *20*, 520-531.
1028 Duan, Z., Andronescu, M., Schutz, K., McIlwain, S., Kim, Y.J., Lee, C., Shendure, J.,
1029 Fields, S., Blau, C.A., and Noble, W.S. (2010). A three-dimensional model of the yeast
1030 genome. Nature *465*, 363-367.
1031 Dubey, R.N., and Gartenberg, M.R. (2007). A tDNA establishes cohesion of a
1032 neighboring silent chromatin domain. Genes Dev *21*, 2150-2160.
1033 Dujon, B. (1996). The yeast genome project: what did we learn? Trends in Genet. *12*,
1034 263-270.
1035 Ebersole, T., Kim, J.H., Samoshkin, A., Kouprina, N., Pavlicek, A., White, R.J., and
1036 Larionov, V. (2011). tRNA genes protect a reporter gene from epigenetic silencing in
1037 mouse cells. Cell Cycle *10*, 2779-2791.
1038 Fabre, E., and Spichal, M. (2014). Subnuclear Architecture of telomeres and
1039 subtelomeres in yeast. In SubTelomeres, E.J. Louis, and M.M. Becker, eds. (Springer),
1040 pp. 13-37.
1041 Fourel, G., Lebrun, E., and Gilson, E. (2002). Protosilencers as building blocks for
1042 heterochromatin. Bioessays *24*, 828-835.
1043 Frenkel, F.E., Chaley, M.B., Korotkov, E.V., and Skryabin, K.G. (2004). Evolution of
1044 tRNA-like sequences and genome variability. Gene *335*, 57-71.
1045 Fu, Y., Sinha, M., Peterson, C.L., and Weng, Z. (2008). The insulator binding protein
1046 CTCF positions 20 nucleosomes around its binding sites across the human genome.
1047 PLoS Genet *4*, e1000138.
1048 Gartenberg, M.R., Neumann, F.R., Laroche, T., Blaszczyk, M., and Gasser, S.M.
1049 (2004). Sir-mediated repression can occur independently of chromosomal and
1050 subnuclear contexts. Cell *119*, 955-967.
1051 Gartenberg, M.R., and Smith, J.S. (2016). The Nuts and Bolts of Transcriptionally Silent
1052 Chromatin in Saccharomyces cerevisiae. Genetics *203*, 1563-1599.
1053 Gasser, S.M., Hediger, F., Taddei, A., Neumann, F.R., and Gartenberg, M.R. (2004).
1054 The function of telomere clustering in yeast: the circe effect. Cold Spring Harb Symp
1055 Quant Biol *69*, 327-337.
1056 Gehlen, L.R., Gruenert, G., Jones, M.B., Rodley, C.D., Langowski, J., and O'Sullivan,
1057 J.M. (2012). Chromosome positioning and the clustering of functionally related loci in
1058 yeast is driven by chromosomal interactions. Nucleus *3*, 370-383.
1059 Geiduschek, E.P., and Kassavetis, G.A. (2001). The RNA polymerase III transcription
1060 apparatus. J Mol Biol *310*, 1-26.
1061 Gerton, J.L., DeRisi, J., Shroff, R., Lichten, M., Brown, P.O., and Petes, T.D. (2000).
1062 Global mapping of meiotic recombination hotspots and coldspots in the yeast
1063 Saccharomyces cerevisiae. Proc Natl Acad Sci U S A *97*, 11383-11390.

Glynn, E.F., Megee, P.C., Yu, H.G., Mistrot, C., Unal, E., Koshland, D.E., DeRisi, J.L., and Gerton, J.L. (2004). Genome-wide mapping of the cohesin complex in the yeast Saccharomyces cerevisiae. PLoS Biol *2*, E259.

Good, P.D., Kendall, A., Ignatz-Hoover, J., Miller, E.L., Pai, D.A., Rivera, S.R., Carrick, B., and Engelke, D.R. (2013). Silencing near tRNA genes is nucleosome-mediated and distinct from boundary element function. Gene *526*, 7-15.

Goodenbour, J.M., and Pan, T. (2006). Diversity of tRNA genes in eukaryotes. Nucleic Acids Res *34*, 6137-6146.

Guacci, V., Hogan, E., and Koshland, D. (1997). Centromere position in budding yeast: evidence for anaphase A. Mol Biol Cell *8*, 957-972.

Haeusler, R.A., and Engelke, D.R. (2004). Genome organization in three dimensions: thinking outside the line. Cell Cycle *3*, 273-275.

Haeusler, R.A., and Engelke, D.R. (2006). Spatial organization of transcription by RNA polymerase III. Nucleic Acids Res *34*, 4826-4836.

Haeusler, R.A., Pratt-Hyatt, M., Good, P.D., Gipson, T.A., and Engelke, D.R. (2008). Clustering of yeast tRNA genes is mediated by specific association of condensin with tRNA gene transcription complexes. Genes Dev *22*, 2204-2214.

Harismendy, O., Gendrel, C.G., Soularue, P., Gidrol, X., Sentenac, A., Werner, M., and Lefebvre, O. (2003). Genome-wide location of yeast RNA polymerase III transcription machinery. Embo J *22*, 4738-4747.

Hediger, F., Neumann, F.R., Van Houwe, G., Dubrana, K., and Gasser, S.M. (2002). Live Imaging of Telomeres. yKu and Sir Proteins Define Redundant Telomere-Anchoring Pathways in Yeast. Curr Biol *12*, 2076-2089.

Heidinger-Pauli, J.M., Mert, O., Davenport, C., Guacci, V., and Koshland, D. (2010). Systematic reduction of cohesin differentially affects chromosome segregation, condensation, and DNA repair. Curr Biol *20*, 957-963.

Heun, P., Laroche, T., Shimada, K., Furrer, P., and Gasser, S.M. (2001). Chromosome dynamics in the yeast interphase nucleus. Science *294*, 2181-2186.

Ho, C.K., and Abelson, J. (1988). Testing for intron function in the essential Saccharomyces cerevisiae tRNA(SerUCG) gene. J Mol Biol *202*, 667-672.

Hsieh, T.H., Weiner, A., Lajoie, B., Dekker, J., Friedman, N., and Rando, O.J. (2015). Mapping Nucleosome Resolution Chromosome Folding in Yeast by Micro-C. Cell *162*, 108-119.

Hsieh, T.S., Fudenberg, G., Goloborodko, A., and Rando, O.J. (2016). Micro-C XL: assaying chromosome conformation from the nucleosome to the entire genome. Nat Methods *13*, 1009-1011.

Huang, J., and Laurent, B.C. (2004). A Role for the RSC chromatin remodeler in regulating cohesion of sister chromatid arms. Cell Cycle *3*, 973-975.

Ivessa, A.S., Lenzmeier, B.A., Bessler, J.B., Goudsouzian, L.K., Schnakenberg, S.L., and Zakian, V.A. (2003). The Saccharomyces cerevisiae helicase Rrm3p facilitates replication past nonhistone protein-DNA complexes. Mol Cell *12*, 1525-1536.

Iwasaki, O., and Noma, K. (2012). Global genome organization mediated by RNA polymerase III-transcribed genes in fission yeast. Gene *493*, 195-200.

Iwasaki, O., Tanaka, A., Tanizawa, H., Grewal, S.I., and Noma, K. (2010). Centromeric localization of dispersed Pol III genes in fission yeast. Mol Biol Cell *21*, 254-265.

1109 Jin, Q., Trelles-Sticken, E., Scherthan, H., and Loidl, J. (1998). Yeast nuclei display
1110 prominent centromere clustering that is reduced in nondividing cells and in meiotic
1111 prophase. J Cell Biol *141*, 21-29.
1112 Jin, Q.W., Fuchs, J., and Loidl, J. (2000). Centromere clustering is a major determinant
1113 of yeast interphase nuclear organization. J Cell Sci *113 (Pt 11)*, 1903-1912.
1114 Keogh, M.C., Kim, J.A., Downey, M., Fillingham, J., Chowdhury, D., Harrison, J.C.,
1115 Onishi, M., Datta, N., Galicia, S., Emili, A.*, et al.* (2006). A phosphatase complex that
1116 dephosphorylates gammaH2AX regulates DNA damage checkpoint recovery. Nature
1117 *439*, 497-501.
1118 Kirkland, J., Peterson, M.R., Still, C.B., Brueggemman, L., Dhillon, N., and Kamakaka,
1119 R. (2015). Heterochromatin formation via recruitment of DNA repair proteins. Molecular
1120 Biology of Cell.
1121 Kirkland, J.G., and Kamakaka, R.T. (2013). Long-range heterochromatin association is
1122 mediated by silencing and double-strand DNA break repair proteins. J Cell Biol *201*,
1123 809-826.
1124 Kirkland, J.G., Raab, J.R., and Kamakaka, R.T. (2013). TFIIIC bound DNA elements in
1125 nuclear organization and insulation. Biochim Biophys Acta *1829*, 418-424.
1126 Kitada, T., Schleker, T., Sperling, A.S., Xie, W., Gasser, S.M., and Grunstein, M. (2011).
1127 gammaH2A is a component of yeast heterochromatin required for telomere elongation.
1128 Cell Cycle *10*, 293-300.
1129 Klein, F., Laroche, T., Cardenas, M.E., Hofmann, J.F., Schweizer, D., and Gasser, S.M.
1130 (1992). Localization of RAP1 and topoisomerase II in nuclei and meiotic chromosomes
1131 of yeast. J Cell Biol *117*, 935-948.
1132 Klein, F., Mahr, P., Galova, M., Buonomo, S.B., Michaelis, C., Nairz, K., and Nasmyth,
1133 K. (1999). A central role for cohesins in sister chromatid cohesion, formation of axial
1134 elements, and recombination during yeast meiosis. Cell *98*, 91-103.
1135 Kogut, I., Wang, J., Guacci, V., Mistry, R.K., and Megee, P.C. (2009). The Scc2/Scc4
1136 cohesin loader determines the distribution of cohesin on budding yeast chromosomes.
1137 Genes Dev *23*, 2345-2357.
1138 Korde, A., Rosselot, J.M., and Donze, D. (2013). Intergenic Transcriptional Interference
1139 Is Blocked by RNA Polymerase III Transcription Factor TFIIIB in Saccharomyces
1140 cerevisiae. Genetics *196*, 427-438.
1141 Laloraya, S., Guacci, V., and Koshland, D. (2000). Chromosomal addresses of the
1142 cohesin component Mcd1p. J Cell Biol *151*, 1047-1056.
1143 Langmead, B., and Salzberg, S.L. (2012). Fast gapped-read alignment with Bowtie 2.
1144 Nat Methods *9*, 357-359.
1145 Lebrun, E., Revardel, E., Boscheron, C., Li, R., Gilson, E., and Fourel, G. (2001).
1146 Protosilencers in Saccharomyces cerevisiae subtelomeric regions. Genetics *158*, 167-
1147 176.
1148 Lemoine, F.J., Degtyareva, N.P., Lobachev, K., and Petes, T.D. (2005). Chromosomal
1149 translocations in yeast induced by low levels of DNA polymerase a model for
1150 chromosome fragile sites. Cell *120*, 587-598.
1151 Lengronne, A., Katou, Y., Mori, S., Yokobayashi, S., Kelly, G.P., Itoh, T., Watanabe, Y.,
1152 Shirahige, K., and Uhlmann, F. (2004). Cohesin relocation from sites of chromosomal
1153 loading to places of convergent transcription. Nature *430*, 573-578.

Lindroos, H.B., Strom, L., Itoh, T., Katou, Y., Shirahige, K., and Sjogren, C. (2006). Chromosomal association of the Smc5/6 complex reveals that it functions in differently regulated pathways. Mol Cell *22*, 755-767.

Lopez-Serra, L., Kelly, G., Patel, H., Stewart, A., and Uhlmann, F. (2014). The Scc2-Scc4 complex acts in sister chromatid cohesion and transcriptional regulation by maintaining nucleosome-free regions. Nat Genet *46*, 1147-1151.

Mano, Y., Kobayashi, T.J., Nakayama, J., Uchida, H., and Oki, M. (2013). Single cell visualization of yeast gene expression shows correlation of epigenetic switching between multiple heterochromatic regions through multiple generations. PLoS Biol *11*, e1001601.

Mekhail, K., Seebacher, J., Gygi, S.P., and Moazed, D. (2008). Role for perinuclear chromosome tethering in maintenance of genome stability. Nature *456*, 667-670.

Mercy, G., Mozziconacci, J., Scolari, V.F., Yang, K., Zhao, G., Thierry, A., Luo, Y., Mitchell, L.A., Shen, M., Shen, Y.*, et al.* (2017). 3D organization of synthetic and scrambled chromosomes. Science *355*.

Miele, A., Bystricky, K., and Dekker, J. (2009). Yeast silent mating type loci form heterochromatic clusters through silencer protein-dependent long-range interactions. PLoS Genet *5*, e1000478.

Mine-Hattab, J., and Rothstein, R. (2012). Increased chromosome mobility facilitates homology search during recombination. Nat Cell Biol.

Moqtaderi, Z., and Struhl, K. (2004). Genome-wide occupancy profile of the RNA polymerase III machinery in Saccharomyces cerevisiae reveals loci with incomplete transcription complexes. Mol Cell Biol *24*, 4118-4127.

Nagarajavel, V., Iben, J.R., Howard, B.H., Maraia, R.J., and Clark, D.J. (2013). Global 'bootprinting' reveals the elastic architecture of the yeast TFIIIB-TFIIIC transcription complex in vivo. Nucleic Acids Res *41*, 8135-8143.

Noma, K., Cam, H.P., Maraia, R.J., and Grewal, S.I. (2006). A role for TFIIIC transcription factor complex in genome organization. Cell *125*, 859-872.

Noma, K.I. (2017). The Yeast Genomes in Three Dimensions: Mechanisms and Functions. Annu Rev Genet.

Oakes, M., Aris, J.P., Brockenbrough, J.S., Wai, H., Vu, L., and Nomura, M. (1998). Mutational analysis of the structure and localization of the nucleolus in the yeast Saccharomyces cerevisiae. J Cell Biol *143*, 23-34.

Ocampo, J., Chereji, R.V., Eriksson, P.R., and Clark, D.J. (2016). The ISW1 and CHD1 ATP-dependent chromatin remodelers compete to set nucleosome spacing in vivo. Nucleic Acids Res *44*, 4625-4635.

Oki, M., and Kamakaka, R.T. (2005). Barrier Function at HMR. Mol Cell *19*, 707-716.

Palladino, F., Laroche, T., Gilson, E., Axelrod, A., Pillus, L., and Gasser, S.M. (1993a). SIR3 and SIR4 proteins are required for the positioning and integrity of yeast telomeres. Cell *75*, 543-555.

Palladino, F., Laroche, T., Gilson, E., Pillus, L., and Gasser, S.M. (1993b). The positioning of yeast telomeres depends on SIR3, SIR4, and the integrity of the nuclear membrane. Cold Spring Harb Symp Quant Biol *58*, 733-746.

Parnell, T.J., Huff, J.T., and Cairns, B.R. (2008). RSC regulates nucleosome positioning at Pol II genes and density at Pol III genes. Embo J *27*, 100-110.

1199 Pimentel, H., Bray, N.L., Puente, S., Melsted, P., and Pachter, L. (2017). Differential
1200 analysis of RNA-seq incorporating quantification uncertainty. Nat Methods *14*, 687-690.
1201 Pombo, A., Jackson, D.A., Hollinshead, M., Wang, Z., Roeder, R.G., and Cook, P.R.
1202 (1999). Regional specialization in human nuclei: visualization of discrete sites of
1203 transcription by RNA polymerase III. Embo J *18*, 2241-2253.
1204 Raab, J.R., Chiu, J., Zhu, J., Katzman, S., Kurukuti, S., Wade, P.A., Haussler, D., and
1205 Kamakaka, R.T. (2012). Human tRNA genes function as chromatin insulators. EMBO J
1206 *31*, 330-350.
1207 Raab, J.R., and Kamakaka, R.T. (2010). Insulators and promoters: closer than we think.
1208 Nat Rev Genet *11*, 439-446.
1209 Roberts, D.N., Stewart, A.J., Huff, J.T., and Cairns, B.R. (2003). The RNA polymerase
1210 III transcriptome revealed by genome-wide localization and activity-occupancy
1211 relationships. Proc Natl Acad Sci U S A *100*, 14695-14700.
1212 Ruben, G.J., Kirkland, J.G., Macdonough, T., Chen, M., Dubey, R.N., Gartenberg, M.R.,
1213 and Kamakaka, R.T. (2011). Nucleoporin Mediated Nuclear Positioning and Silencing of
1214 HMR. PLoS One *6*, e21923.
1215 Schober, H., Ferreira, H., Kalck, V., Gehlen, L.R., and Gasser, S.M. (2009). Yeast
1216 telomerase and the SUN domain protein Mps3 anchor telomeres and repress
1217 subtelomeric recombination. Genes Dev *23*, 928-938.
1218 Schramm, L., and Hernandez, N. (2002). Recruitment of RNA polymerase III to its
1219 target promoters. Genes Dev *16*, 2593-2620.
1220 Sharp, P.M., and Lloyd, A.T. (1993). Regional base composition variation along yeast
1221 chromosome III: evolution of chromosome primary structure. Nucleic Acids Res *21*, 179-
1222 183.
1223 Simms, T.A., Dugas, S.L., Gremillion, J.C., Ibos, M.E., Dandurand, M.N., Toliver, T.T.,
1224 Edwards, D.J., and Donze, D. (2008). TFIIIC binding sites function as both
1225 heterochromatin barriers and chromatin insulators in Saccharomyces cerevisiae.
1226 Eukaryot Cell *7*, 2078-2086.
1227 Simms, T.A., Miller, E.C., Buisson, N.P., Jambunathan, N., and Donze, D. (2004). The
1228 Saccharomyces cerevisiae TRT2 tRNAThr gene upstream of STE6 is a barrier to
1229 repression in MATalpha cells and exerts a potential tRNA position effect in MATa cells.
1230 Nucleic Acids Res *32*, 5206-5213.
1231 Snider, C.E., Stephens, A.D., Kirkland, J.G., Hamdani, O., Kamakaka, R.T., and Bloom,
1232 K. (2014). Dyskerin, tRNA genes, and condensin tether pericentric chromatin to the
1233 spindle axis in mitosis. J Cell Biol *207*, 189-199.
1234 Szilard, R.K., Jacques, P.E., Laramee, L., Cheng, B., Galicia, S., Bataille, A.R., Yeung,
1235 M., Mendez, M., Bergeron, M., Robert, F.*, et al.* (2010). Systematic identification of
1236 fragile sites via genome-wide location analysis of gamma-H2AX. Nat Struct Mol Biol *17*,
1237 299-305.
1238 Taddei, A., Gartenberg, M.R., Neumann, F.R., Hediger, F., and Gasser, S.M. (2005).
1239 Multiple pathways tether telomeres and silent chromatin at the nuclear periphery:
1240 functional implications for sir-mediated repression. Novartis Found Symp *264*, 140-156;
1241 discussion 156-165, 227-130.
1242 Taddei, A., and Gasser, S.M. (2004). Multiple pathways for telomere tethering:
1243 functional implications of subnuclear position for heterochromatin formation. Biochim
1244 Biophys Acta *1677*, 120-128.

Taddei, A., Hediger, F., Neumann, F.R., Bauer, C., and Gasser, S.M. (2004). Separation of silencing from perinuclear anchoring functions in yeast Ku80, Sir4 and Esc1 proteins. Embo J *23*, 1301-1312.

Taddei, A., Schober, H., and Gasser, S.M. (2010). The budding yeast nucleus. Cold Spring Harb Perspect Biol *2*, a000612.

Taddei, A., Van Houwe, G., Hediger, F., Kalck, V., Cubizolles, F., Schober, H., and Gasser, S.M. (2006). Nuclear pore association confers optimal expression levels for an inducible yeast gene. Nature *441*, 774-778.

Therizols, P., Duong, T., Dujon, B., Zimmer, C., and Fabre, E. (2010). Chromosome arm length and nuclear constraints determine the dynamic relationship of yeast subtelomeres. Proc Natl Acad Sci U S A *107*, 2025-2030.

Thompson, M., Haeusler, R.A., Good, P.D., and Engelke, D.R. (2003). Nucleolar clustering of dispersed tRNA genes. Science *302*, 1399-1401.

Tjong, H., Gong, K., Chen, L., and Alber, F. (2012). Physical tethering and volume exclusion determine higher-order genome organization in budding yeast. Genome Res *22*, 1295-1305.

Uhlmann, F. (2016). SMC complexes: from DNA to chromosomes. Nat Rev Mol Cell Biol *17*, 399-412.

Valenzuela, L., Dhillon, N., Dubey, R.N., Gartenberg, M.R., and Kamakaka, R.T. (2008). Long-range communication between the silencers of HMR. Mol Cell Biol *28*, 1924-1935.

Valenzuela, L., Gangadharan, S., and Kamakaka, R.T. (2006). Analyses of SUM1-1-mediated long-range repression. Genetics *172*, 99-112.

Van Bortle, K., and Corces, V.G. (2012). tDNA insulators and the emerging role of TFIIIC in genome organization. Transcription *3*, 277-284.

Van Bortle, K., Nichols, M.H., Li, L., Ong, C.T., Takenaka, N., Qin, Z.S., and Corces, V.G. (2014). Insulator function and topological domain border strength scale with architectural protein occupancy. Genome Biol *15*, R82.

Verdaasdonk, J.S., Vasquez, P.A., Barry, R.M., Barry, T., Goodwin, S., Forest, M.G., and Bloom, K. (2013). Centromere tethering confines chromosome domains. Mol Cell *52*, 819-831.

Wang, J., Lunyak, V.V., and Jordan, I.K. (2012). Genome-wide prediction and analysis of human chromatin boundary elements. Nucleic Acids Res *40*, 511-529.

Wang, Y., Vujcic, M., and Kowalski, D. (2001). DNA replication forks pause at silent origins near the HML locus in budding yeast. Mol Cell Biol *21*, 4938-4948.

Weiner, A., Hughes, A., Yassour, M., Rando, O.J., and Friedman, N. (2010). High-resolution nucleosome mapping reveals transcription-dependent promoter packaging. Genome Res *20*, 90-100.

Withers, M., Wernisch, L., and dos Reis, M. (2006). Archaeology and evolution of transfer RNA genes in the Escherichia coli genome. Rna *12*, 933-942.

Yuan, G.C., Liu, Y.J., Dion, M.F., Slack, M.D., Wu, L.F., Altschuler, S.J., and Rando, O.J. (2005). Genome-scale identification of nucleosome positions in S. cerevisiae. Science *309*, 626-630.

Zimmer, C., and Fabre, E. (2011). Principles of chromosomal organization: lessons from yeast. J Cell Biol *192*, 723-733.

Figure1

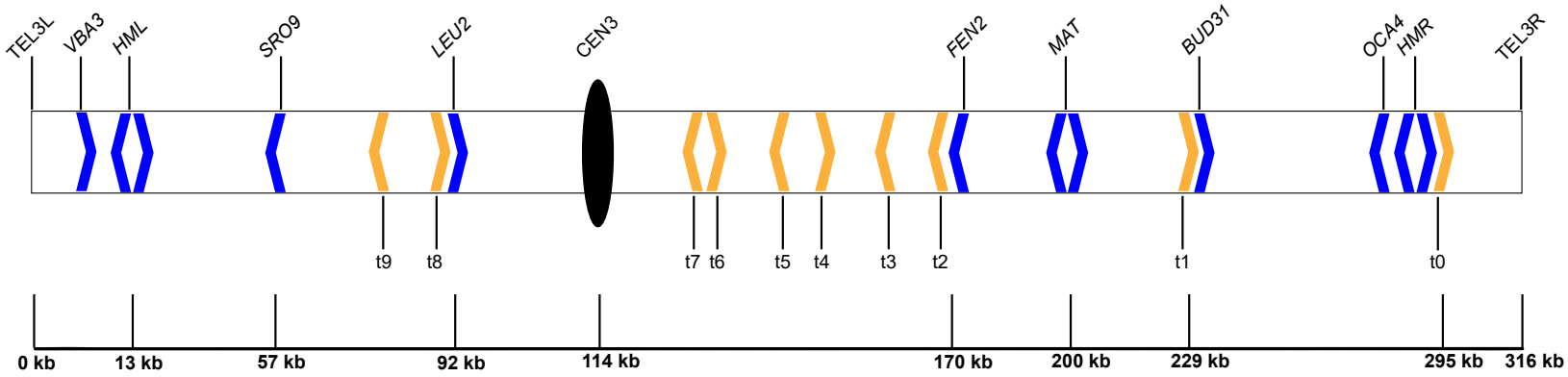
TEL3L
VBA3
HML
SRO9
LEU2
CEN3
FEN2
MAT
BUD31
OCA4
HMR
TEL3R
t9
t8
t7
t6
t5
t4
t3
t2
t1
t0
0 kb
13 kb
57 kb
92 kb
114 kb
170 kb
200 kb
229 kb
295 kb
316 kb

Figure 2

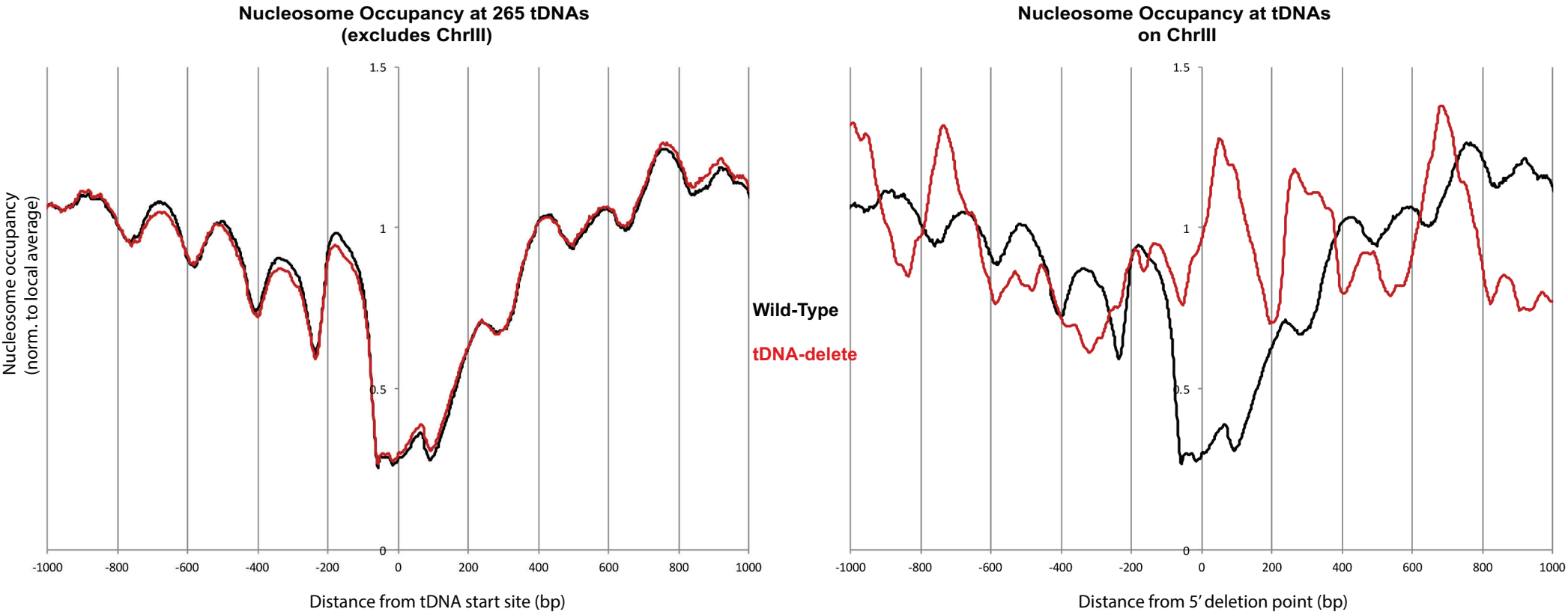
Nucleosome Occupancy at 265 tDNAs
(excludes ChrIII)
Nucleosome occupancy
(norm. to local average)
1.5
1
0.5
0
-1000
-800
-600
-400
-200
0
200
400
600
800
1000
Distance from tDNA start site (bp)
Wild-Type
tDNA-delete
Nucleosome Occupancy at tDNAs
on ChrIII
1.5
1
0.5
0
-1000
-800
-600
-400
-200
0
200
400
600
800
1000
Distance from 5′ deletion point (bp)

Figure 3

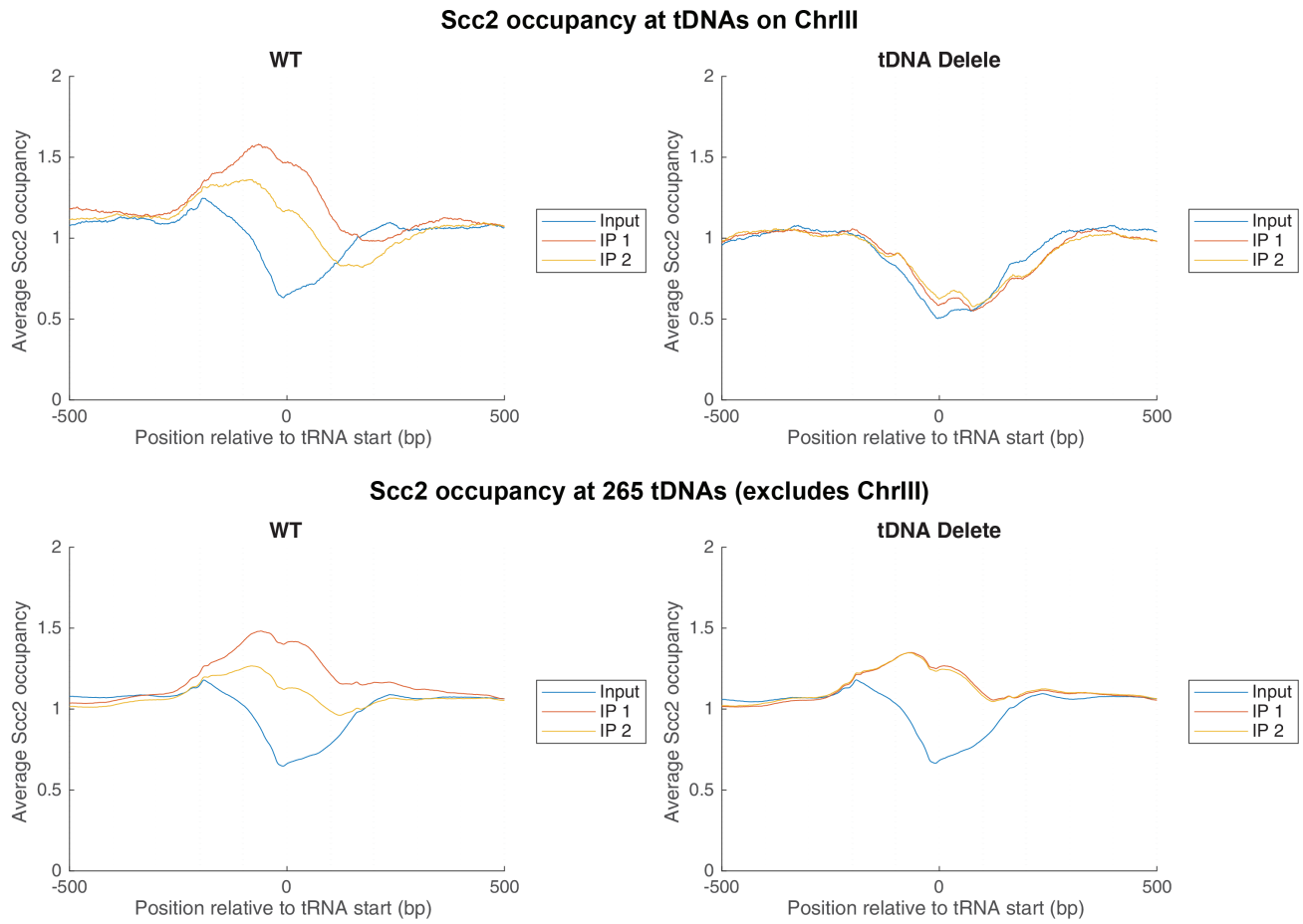

Figure 4A

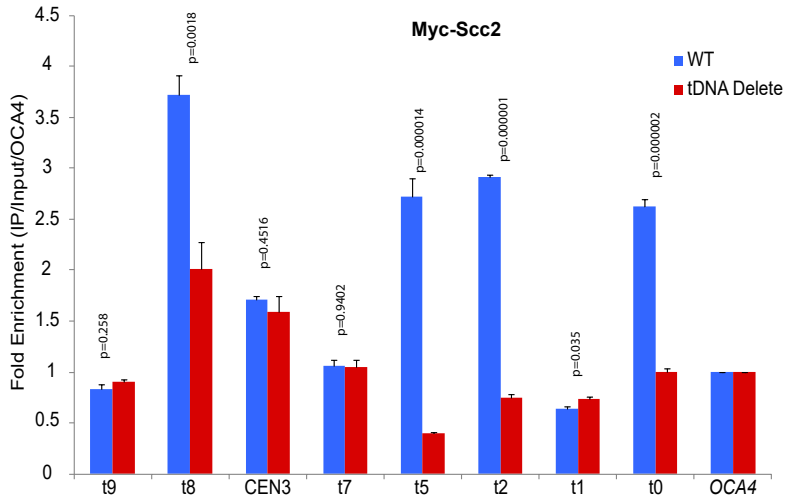

Figure 4B

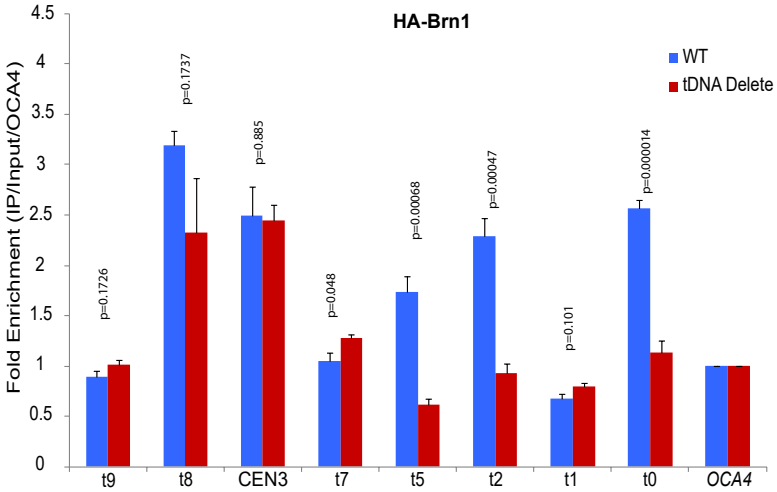

Figure 5

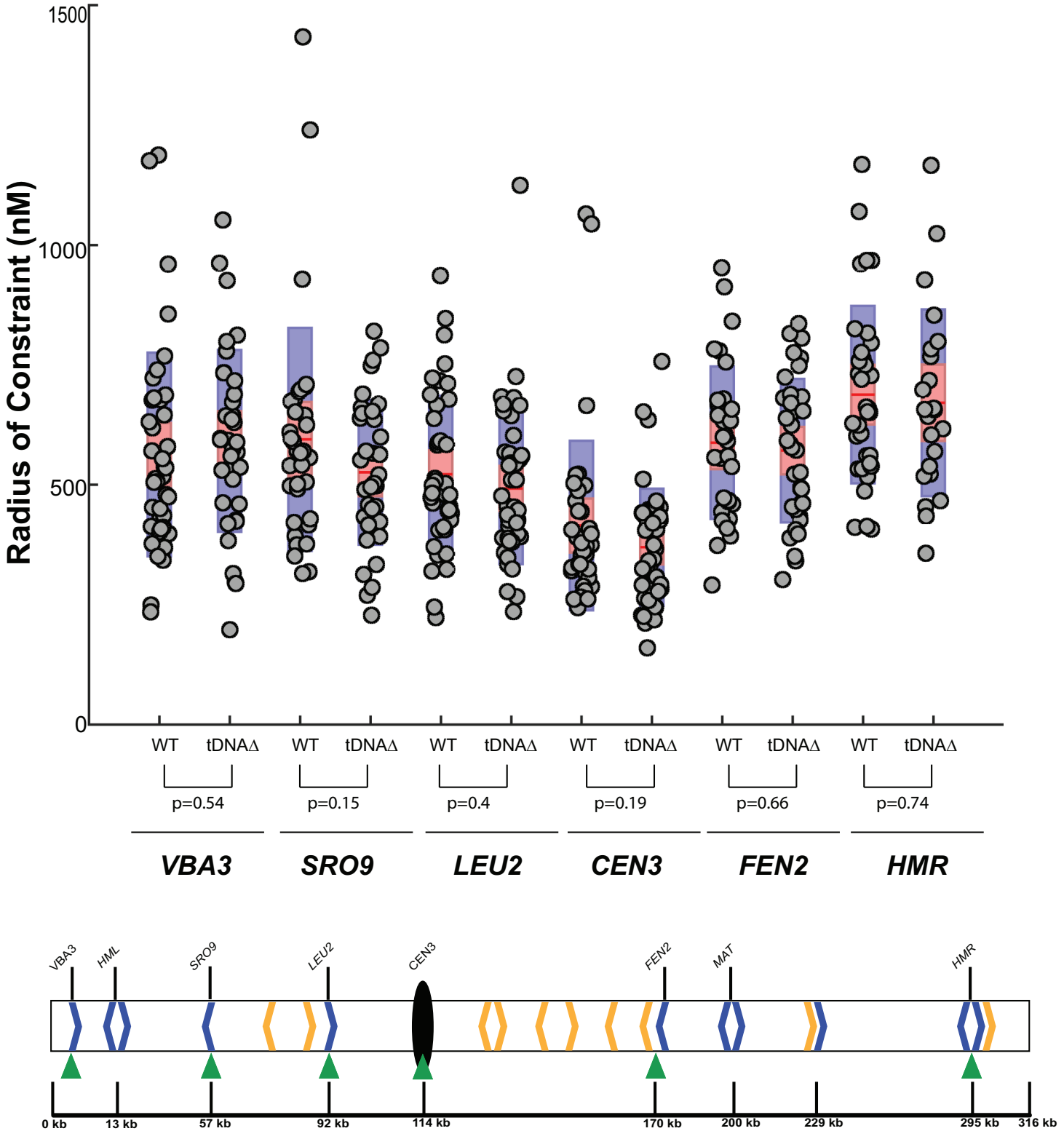
Radius of Constraint (nM)
1500
1000
500
0
WT
tDNAΔ
p=0.54
p=0.15
p=0.4
p=0.19
p=0.66
p=0.74
VBA3
SRO9
LEU2
CEN3
FEN2
HMR
VBA3
HML
SRO9
LEU2
CEN3
FEN2
MAT
HMR
0 kb
13 kb
57 kb
92 kb
114 kb
170 kb
200 kb
229 kb
295 kb
316 kb

Figure 6

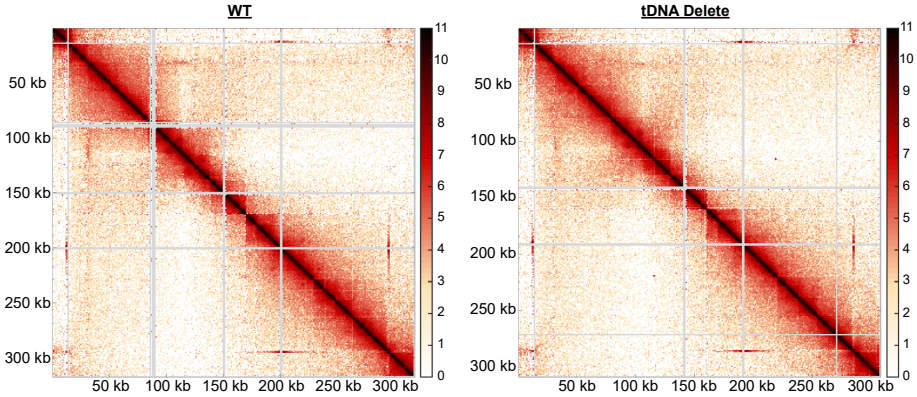
WT
tDNA Delete
50 kb
100 kb
150 kb
200 kb
250 kb
300 kb
0
1
2
3
4
5
6
7
8
9
10
11

Figure 7A

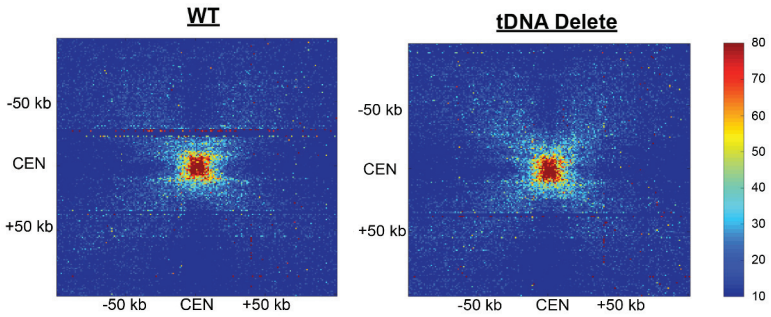

Figure 7B

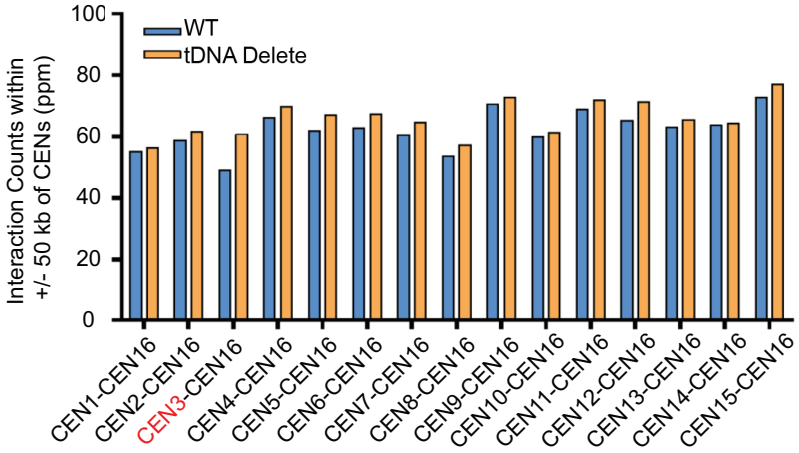

Figure 7C

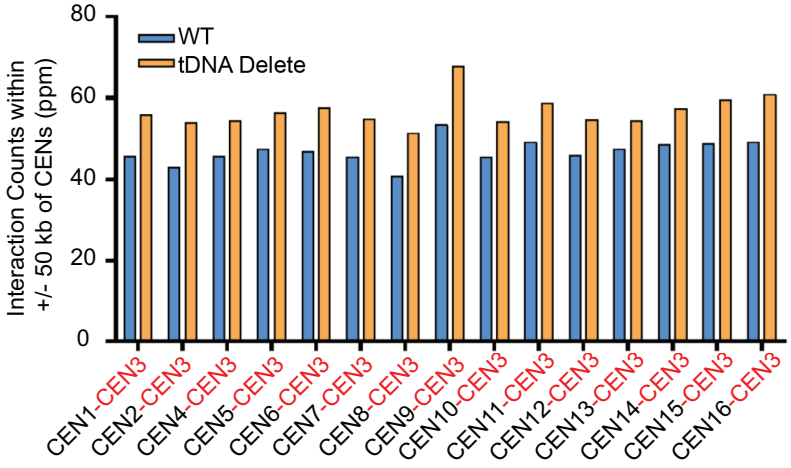

Figure 8A

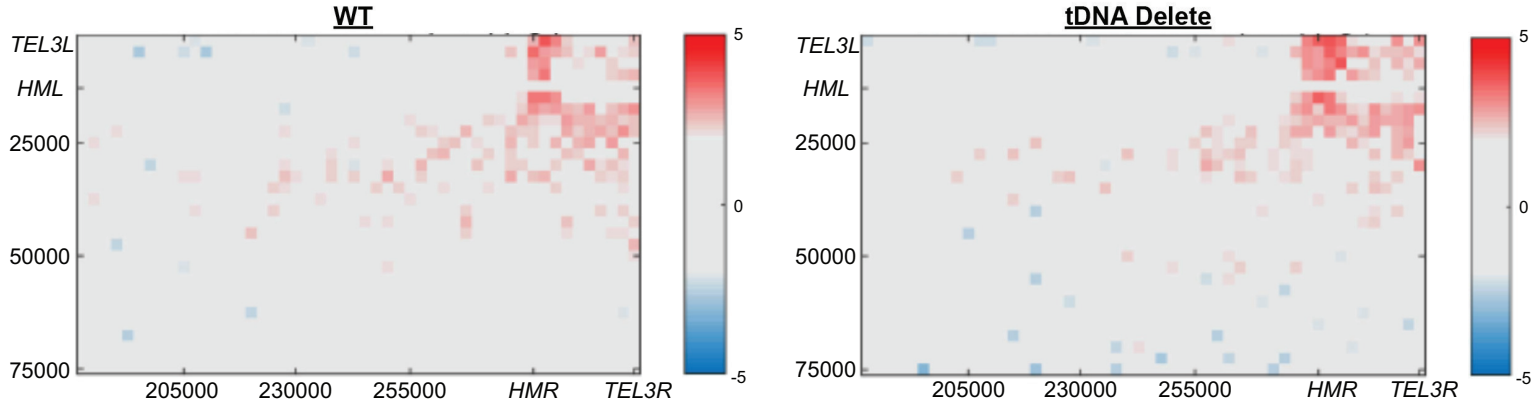

Figure 8B.

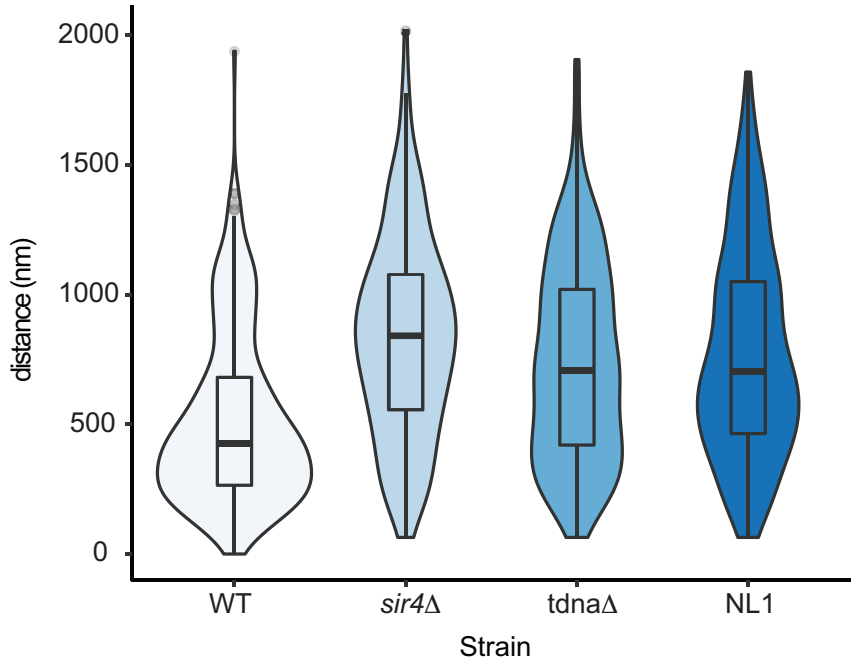

Figure 8C

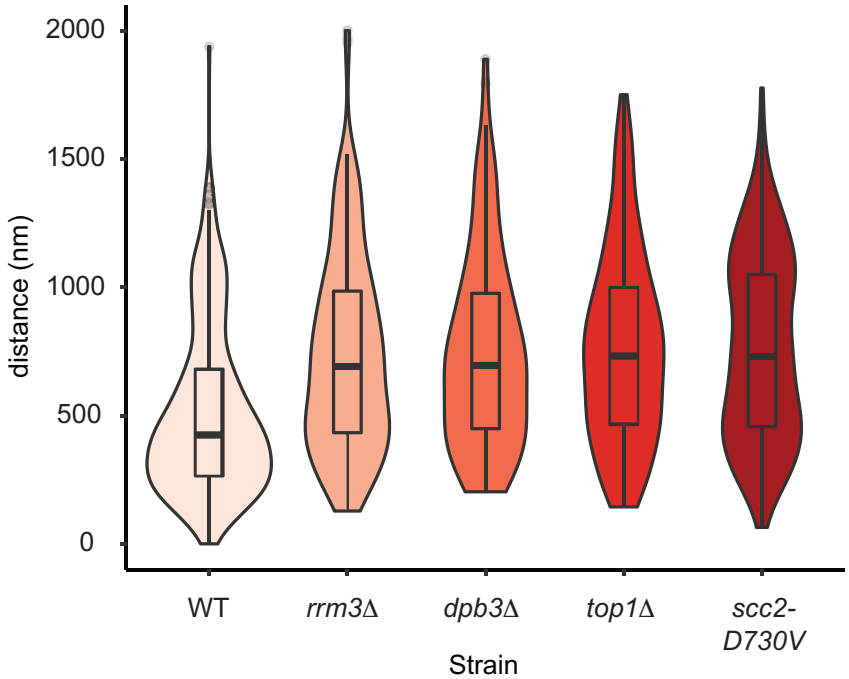

Figure 9A

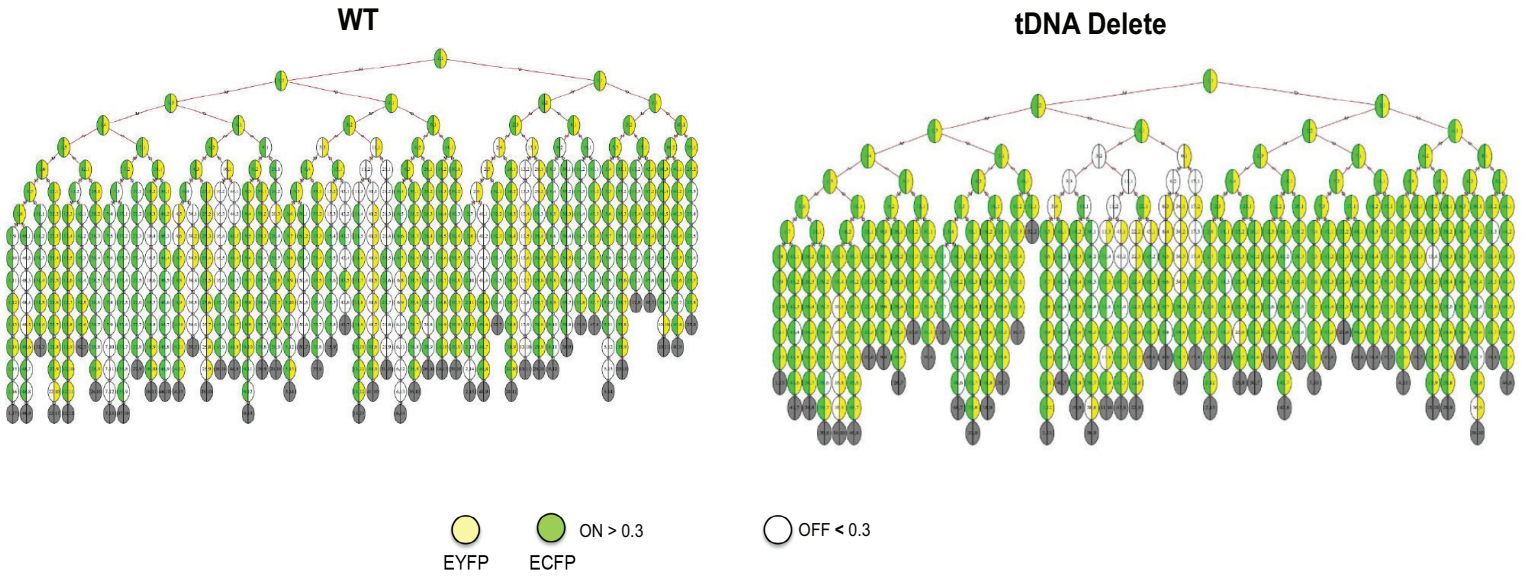

Figure 9B

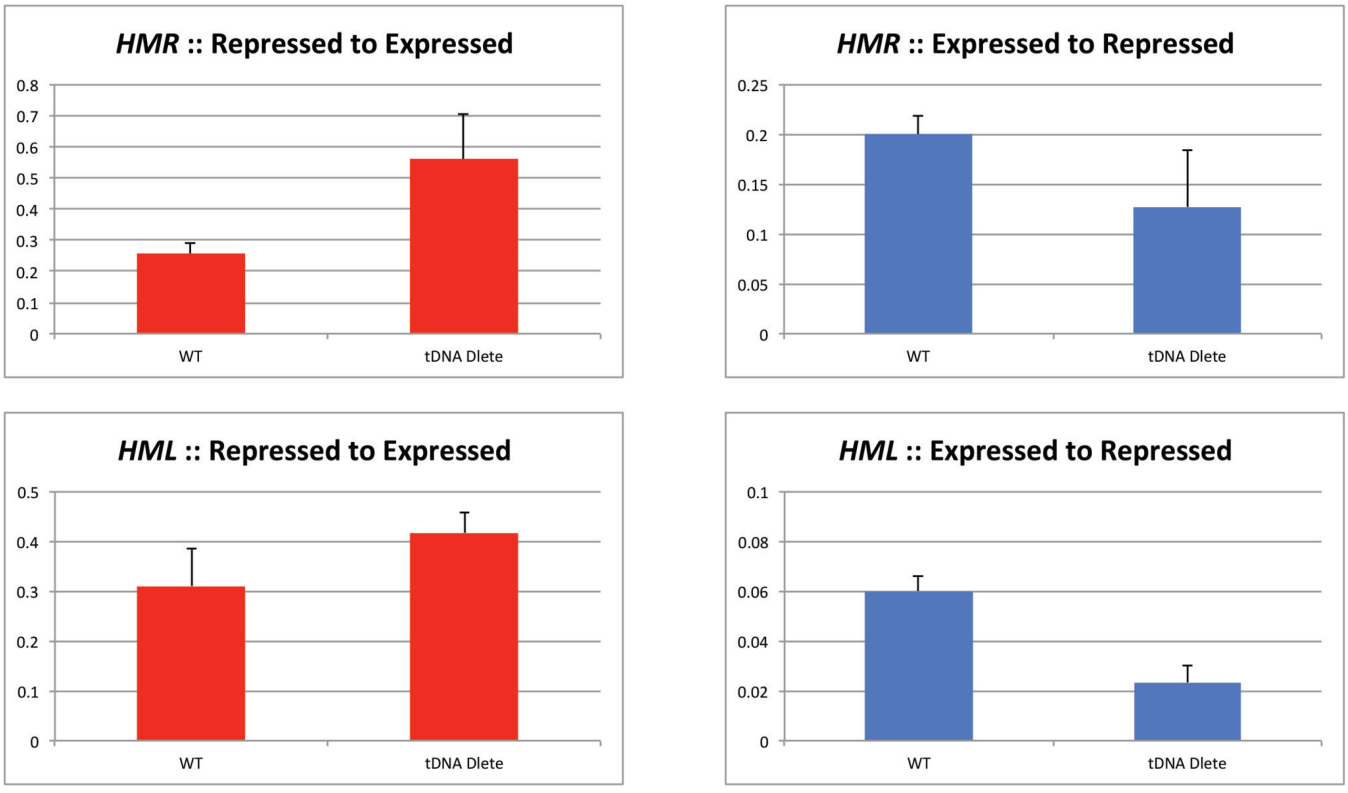

Upregulated in tDNA del	q-Val (likelihood ratio test)	q val (Wald test)	beta statistic
YCR061w	0.042003857	3.22E-11	0.6580998
YDL124w	0.042003857	6.31E-14	0.4395261
YHR214c-B	0.005672182	2.35E-210	2.5870238
YNL160w	0.040272092	2.69E-20	0.5348964
YOR201c	0.020396347	9.18E-27	0.7685378
YOR202w	0.009117145	1.20E-76	3.7326308
YPL240c	0.042003857	1.20E-15	0.5188043

Downregulated	q-Val (likelihood ratio test)	q val (Wald test)	beta statistic
YBR068c	0.030966243	1.53E-20	-0.5156825
YBR296c	0.039894621	1.87E-19	-0.5692597
YCR008w	0.015662463	6.48E-43	-1.1217
YER073w	0.045197971	8.81E-16	-0.5691673
YER091c	0.042003857	1.79E-20	-0.5345605
YGL009c	0.009117145	1.47E-82	-2.0202761
YHR208w	0.007776891	7.72E-106	-1.3235331
YJR010w	0.042003857	3.34E-13	-0.8073784
YJR016c	0.017736878	3.09E-29	-0.5823368
YKL030w	0.042003857	3.46E-11	-0.6718075
YKL120w	0.007776891	1.47E-94	-1.4546702
YLR355c	0.042003857	2.35E-12	-0.387429
YMR108w	0.042003857	3.72E-15	-0.4213145
YOR271c	0.027535084	4.63E-26	-0.5903308